JPET Fast Forward. Published on June 29, 2017 as DOI: 10.1124/jpet.117.241596
This article has not been copyedited and formatted. The final version may differ from this version.

The use of physiology-based PK and PD modeling in the discovery of the dual orexin receptor antagonist ACT-541468

Alexander Treiber, Ruben de Kanter, Catherine Roch, John Gatfield, Christoph Boss, Markus von Raumer, Benno Schindelholz, Clemens Mühlan, Joop van Gerven, Francois Jenck

Departments of Preclinical Drug Metabolism and Pharmacokinetics *(A.T., R.d.K.)*, Preclinical Pharmacology *(C.R, F.J.)*, Biology *(J.G.)*, Chemistry *(C.B.)*, Clinical Pharmacology *(C.M.)* and Preclinical Development *(B.S., M.v.R.)*, Idorsia Pharmaceuticals Ltd, Allschwil, Switzerland. Center for Human Drug Research, Leiden, The Netherlands *(J.v.G)*.

JPET Fast Forward. Published on June 29, 2017 as DOI: 10.1124/jpet.117.241596
This article has not been copyedited and formatted. The final version may differ from this version.

Running title: Role of physiology-based modeling in ACT-541468 discovery

Corresponding author: Alexander Treiber

Idorsia Pharmaceuticals Ltd

Hegenheimermattweg 91

4123 Allschwil

Switzerland

+41 61 565 65 92 (phone)

+41 61 565 89 03 (fax)

alexander.treiber@idorsia.com

Text pages: 46

Number of tables: 8

Number of figures: 10

Number of references: 67

Abstract: 250 words

Introduction: 817 words

Discussion: 1630 words

Recommended section assignment: Drug Discovery and Translational Medicine, Neuropharmacology

Abbreviations: ADAM, advanced dissolution, absorption, and metabolism; ADME, absorption, distribution, metabolism, and excretion; AMS, accelerator mass spectrometry; ANOVA, analysis of variance; AUC, area under the plasma concentration vs. time curve; $AUC_{0\text{-}inf}$, area under the plasma concentration vs. time curve extrapolated to infinity; $AUC_{0\text{-}last}$, area under the plasma concentration vs. time curve up to the last measurable

concentration; CHO, Chinese hamster ovary; CL, total plasma clearance; CL_{int}, intrinsic clearance; C_{max}, peak observed plasma concentration; CRC, concentration-response curve; DMF, dimethylformamide; DMSO, dimethyl sulfoxide; DORA, dual orexin receptor antagonist; EEG, electroencephalographic; EMG, electromyographic; F, oral bioavailability; FaSSIF, fasted state stimulated intestinal fluid; FCS, fetal calf serum; FeSSIF, fed state stimulated intestinal fluid; $f_{u,brain}$, fraction unbound in the brain; $f_{u,gut}$, fraction unbound in the gut; $f_{u,mic}$, fraction unbound in liver microsomes; $f_{u,OX2assay}$, fraction unbound in OX_2 binding assay; $f_{u,plasma}$, fraction unbound in plasma; HATU, O-(7-azabenzotriazol-1-yl)-N,N,N′,N′-tetramethyluronium-hexafluorphosphate; HBSS, Hank´s buffered saline solution; HPLC, high performance liquid chromatography; HPβCD, 2-hydroxypropyl-β-cyclodextrin; K_b, inhibition constant as determined by a functional assay; K_p, tissue to plasma partition coefficient; LC-MS/MS, liquid chromatography coupled to mass spectrometry; logD, distribution coefficient; MDCK-II, Madin-Darby canine kidney (cell line); OAT, organic anion transporter, OX_1, orexin-1 receptor; OX_2, orexin-2 receptor; OxA, orexin A; PBPK-PD, physiology-based pharmacokinetic and pharmacodynamic (modeling); PD, pharmacodynamic; PK, pharmacokinetic; (non-)REM, (non-)rapid eye movement; RFU, relative fluorescence units; $ROt_{1/2}$, receptor occupancy half-life; RT, room temperature; $T_{1/2}$, half-life; T_{max}, time to reach peak plasma concentration; V_{ss}, apparent volume of distribution at steady-state; σ_g, geometric standard deviation.

JPET Fast Forward. Published on June 29, 2017 as DOI: 10.1124/jpet.117.241596
This article has not been copyedited and formatted. The final version may differ from this version.

ABSTRACT

The identification of new sleep drugs poses particular challenges in drug discovery due to disease-specific requirements such as rapid onset of action, sleep maintenance throughout major parts of the night, and absence of residual next-day effects. Robust tools to estimate drug levels in human brain are therefore key for a successful discovery program. Animal models constitute an appropriate choice for drugs without species differences in receptor pharmacology or pharmacokinetics. Translation to man becomes more challenging in case inter-species differences are prominent. This report describes the discovery of the dual OX_1 and OX_2 receptor antagonist ACT-541468 out of a class of structurally related compounds by use of physiology-based pharmacokinetic and pharmacodynamic (PBPK-PD) modeling applied already early in drug discovery. While all drug candidates exhibited similar target receptor potencies and efficacy in a rat sleep model, they exhibited large inter-species differences in key factors determining their pharmacokinetic profile. Human PK models were built based on in vitro metabolism and physico-chemical data, and were then used to predict the time course of OX2 receptor occupancy in brain. An active ACT-541468 dose of 25 mg was estimated based on OX_2 receptor occupancy thresholds of about 65% derived from clinical data of two other orexin antagonists, almorexant and suvorexant. Modeling predictions for ACT-541468 in man were largely confirmed in a single-ascending dose trial in healthy subjects. PBPK-PD modeling applied early in drug discovery therefore has great potential to assist in the identification of drug molecules when specific pharmacokinetic and pharmacodynamic requirements need to be met.

INTRODUCTION

Insomnia, characterized by difficulties with sleep onset and/or sleep maintenance, affects 10–15% of the population chronically, with additional 15–20% suffering from it occasionally. Insomnia has a wide range of effects on quality of life and is associated with increased accident risk and chronic health problems (Zammit, 2007). Historically, insomnia treatments have targeted GABA-A, histamine, serotonin or melatonin receptors. GABA-A receptor modulators such as zolpidem, which currently dominate the market, tend to increase non-rapid eye movement (non-REM) sleep and decrease REM sleep compared with normal sleep architecture (Bettica et al., 2012b). This may be the reason for the observed decrease in cognitive performance and locomotor skills when walking during nighttime awakening (Otmani et al., 2008; Frey et al., 2011), the latter being of particular concern for the elderly (Glass et al., 2005).

The orexin system was discovered in the late 1990s (de Lecea et al., 1998; Sakurai, 1999) and is comprised of two peptides, orexin A (OxA) and orexin B, produced in a small number of neurons in the lateral hypothalamus, and two G protein-coupled receptors, orexin-1 (OX_1) and orexin-2 (OX_2), widely expressed throughout the brain. Orexin deficiency has been linked to human narcolepsy/cataplexy, a neurological disorder in which patients suffer from an uncontrolled sleep-wake cycle (Peyron et al., 2000; Thannickal et al., 2000). This indicates that the orexin system plays an essential role in promoting alertness and maintaining wakefulness under motivational circumstances. It supports behavioral and physiological adaptation to relevant internal and external environmental stimuli such as physiological need state, exposure to threats or reward opportunities (Sakurai, 2007; Carter et al., 2009; Tsujino and Sakurai, 2009; Mahler et al., 2014).

JPET Fast Forward. Published on June 29, 2017 as DOI: 10.1124/jpet.117.241596
This article has not been copyedited and formatted. The final version may differ from this version.

With the discovery of potent low molecular weight compounds, orexin receptor antagonism has emerged as a novel concept for the treatment of insomnia disorders. Unlike classical hypnotics targeting GABA-A, histamine or serotonin receptors, orexin receptor antagonists promote sleep in a distinct manner as they maintain a natural sleep architecture and do not impair cognitive function or locomotor skills (Hoever et al., 2012b; Ramirez et al., 2013; Tannenbaum et al., 2016).

Both, dual orexin receptor antagonists (DORAs) including almorexant (Hoever et al., 2012b), suvorexant (Herring et al., 2012), filorexant (Connor et al., 2016), lemborexant (Yoshida et al., 2015) and SB-649868 (Bettica et al., 2012a), as well as the OX_2-selective antagonist seltorexant have been tested in insomnia patients (Bonaventure et al., 2015a). Polysomnography in animals and healthy human subjects suggest a qualitatively comparable sleep-promoting profile for both DORAs and OX_2-selective compounds, although relative impact on REM vs. non-REM sleep may differ (Dugovic et al., 2014; Jacobson et al., 2016). Comparative studies with DORAs and OX_2-selective compounds indicate that higher OX_2 receptor occupancies are required by OX_2-selective compounds (Mieda et al., 2011; Gotter et al., 2016), as recently shown with the DORA filorexant and the OX_2-selective MK-1064. As OX_1-selective antagonists alone lack sleep-promoting efficacy (Gozzi et al., 2011), the overall data suggest a complementary role of OX_1 antagonism in the sleep-promoting efficacy of DORAs. OX_1 receptors also appear to play an essential role in anxiety states (Merlo Pich and Melotto, 2014), and OX_1-selective antagonists additionally attenuate behavioral and cardiovascular responses to stress without altering baseline motor or autonomic functions (Gozzi et al., 2011; Johnson et al., 2012; Bonaventure et al., 2015b).

In 2014, suvorexant was approved in the USA under the trade name Belsomra for the treatment of insomnia. During regulatory review, the Food and Drug Administration expressed concerns about potential next-day residual effects (Citrome, 2014; Vermeeren et

al., 2015) associated with higher Belsomra doses as a consequence of its extended plasma half-life. This episode highlights the importance of identifying compounds with an optimal pharmacokinetic and pharmacodynamic (PK/PD) profile in man already during the discovery process of an insomnia drug.

From a drug discovery perspective, the identification of candidate molecules for the treatment of insomnia poses particular challenges. Beyond pharmacological target potency and brain penetration as basic requirements, rapid onset and adequate sleep duration are key features. For compounds with little inter-species differences in receptor pharmacology and pharmacokinetics, appropriate drug candidates might be readily identified on the basis of animal pharmacology data. Translational aspects become more important for molecules exhibiting pronounced inter-species differences in drug disposition. For example, plasma protein binding affects drug distribution into tissues and total blood clearance, and thus influences the pharmacokinetic half-life of a drug. Physiology-based pharmacokinetic and pharmacodynamic (PBPK-PD) modeling has been established as an appropriate tool to translate animal PK and PD data into man early in drug development (Jones et al., 2009). The present report describes the central and early role of PBPK-PD modeling in drug discovery as a key tool in the selection process of ACT-541468, a DORA that is currently in phase 2 clinical development for the treatment of insomnia disorders. While this report focuses on only three prototypical compounds, the approach was in fact applied to a set of about 20 structural analogs from the same chemical class.

JPET Fast Forward. Published on June 29, 2017 as DOI: 10.1124/jpet.117.241596
This article has not been copyedited and formatted. The final version may differ from this version.

MATERIALS AND METHODS

Chemicals and reagents

(S)-(2-(5-chloro-4-methyl-1H-benzo[d]imidazol-2-yl)-2-methylpyrrolidin-1-yl)(5-methoxy-2-(2H-1,2,3-triazol-2-yl)phenyl)methanone (ACT-541468), (S)-(2-(5-chloro-1,4-dimethyl-1H-benzo[d]imidazol-2-yl)-2-methylpyrrolidin-1-yl)(5-methyl-2-(2H-1,2,3-triazol-2-yl) phenyl)methanone (ACT-605143), (S)-(2-(6-bromo-4-methyl-1H-benzo[d]imidazol-2-yl)-2-methylpyrrolidin-1-yl)(5-methyl-2-(pyrimidin-2-yl)phenyl)methanone (ACT-658090), almorexant, suvorexant (**Figure 1**), and their corresponding salts were synthesized by the Medicinal Chemistry department of Actelion Pharmaceuticals Ltd (Allschwil, Switzerland) as described in **Supplemental Figure S1**, or according to published methods (Mangion et al., 2012; Boss et al., 2013; Verzijl et al., 2013; Boss et al., 2015a; Boss et al., 2015b). Chemical purity of all compounds was in excess of 97%.

Orexin receptor antagonist assays

OxA curve shift experiments were performed to determine the surmountability of antagonism and to calculate the antagonistic potency (apparent K_b) of the three benzimidazole compounds. Chinese hamster ovary (CHO) cells expressing the human or rat OX_1 or OX_2 receptors were grown in culture medium (Ham's F-12 with L-glutamine, Life Technologies) containing 300 μg/mL (for human receptor-expressing cells) or 1000 μg/mL (for rat receptor-expressing cells) G418, 100 U/mL penicillin, 100 μg/mL streptomycin, and 10% heat-inactivated fetal calf serum (FCS). Prior to the experiment, the cells were seeded at 20,000 cells/well into 384-well black clear-bottom sterile plates (Greiner) and incubated overnight at 37°C in 5% CO_2. On the day of the assay, culture medium in each well was replaced with 50 μL of staining buffer (1× Hank´s buffered saline solution [HBSS], 1% FCS, 20 mM HEPES, 0.375 g/L $NaHCO_3$, 5 mM of the OAT inhibitor probenecid [Sigma], 3 μM

JPET Fast Forward. Published on June 29, 2017 as DOI: 10.1124/jpet.117.241596
This article has not been copyedited and formatted. The final version may differ from this version.

of the fluorogenic calcium indicator fluo-4 AM [Life Technologies], and 10% pluronic® F-127 [Life Technologies]). The cell plates were incubated for 1 h at 37°C in 5% CO_2 followed by equilibration at room temperature (RT) for ≥ 30 min. Fluo-4-stained cells were supplemented with 10 µL of 1:10 serially diluted 6-fold concentrated antagonist solution in the assay buffer (1× HBSS buffer, 0.1% bovine serum albumin, 20 mM HEPES, 0.375 g/L $NaHCO_3$, pH 7.4) containing 0.6% DMSO. After 120 min, cells were stimulated with 10 µL of 1:5 serially diluted 7× OxA solution in assay buffer containing ≤ 0.1% methanol, resulting in final concentrations between 0.01 and 1000 nM. Calcium mobilization (proportional to OX receptor activation by OxA) was measured using the fluorescence imaging plate reader (FLIPR®) assay (Tetra, Molecular Devices; excitation: 470–495 nm; emission: 515–575 nm). To calculate the apparent K_b values, FLIPR traces were subjected to spatial uniformity correction and normalized by trace alignment at the last time point before agonist addition (ScreenWorks software, Molecular Devices). The maximum fluorescence signals per well were used to generate OxA concentration-response curves (CRCs) in GraphPad Prism (GraphPad Software). The EC_{50} values and Hill slopes (n) for the OxA CRCs, and the IC_{50} values of the antagonists at approximately EC_{70} of OxA (1.6 nM for human OX_1 and OX_2, 8 nM for rat OX_1 and OX_2) were calculated using the proprietary IC_{50} Witch software (curve-intrinsic minima and maxima were used). The apparent K_b values were calculated via the generalized Cheng-Prusoff equation, using the on-day OxA EC_{50} value (EC_{50OxA}) and the OxA concentration used for stimulation ($[OxA_{stim}]$), with the following formula (Cheng and Prusoff, 1973; Miller et al., 1999).

$$K_b = \frac{\mathrm{IC_{50}}}{\left(2 + \left(\frac{[\mathrm{OxA_{stim}}]}{\mathrm{EC_{50OxA}}}\right)^n\right)^{\frac{1}{n}} - 1}$$

JPET Fast Forward. Published on June 29, 2017 as DOI: 10.1124/jpet.117.241596
This article has not been copyedited and formatted. The final version may differ from this version.

Approximate receptor occupancy half-lives ($ROt_{1/2}$) of the antagonists were determined using calcium release assays after antagonist wash-out. To this end, fluo-4-stained CHO cells were supplemented with 10 µL of 6× concentrated antagonists (serially diluted 1:10 in assay buffer with 0.6% DMSO). After 120 min, cells were washed extensively with assay buffer and then stimulated at several time points (0 to 63 min) with 10 µL of a 7× OxA solution, giving a final OxA concentration of EC_{70}. Compound incubations and wash-out phase were performed at 37°C. Calcium mobilization was measured, and IC_{50} values were calculated and converted to the apparent K_b values via the generalized Cheng-Prusoff equation, using the OxA CRC slope determined at every time point, as described above (software settings: curve-intrinsic maximum; fixed minimum: full block by 10 µM suvorexant). The geometric means of K_b values generated in three independent experiments were then plotted on a semi-logarithmic scale against time. The $ROt_{1/2}$ was calculated from the K_b values obtained at 0 and 33 min after wash-out, assuming first-order dissociation kinetics, with the following formula:

$$\mathrm{ROt}_{1/2} = \frac{33\ min}{\log_2\left(\frac{K_{b\ 33\ min}}{K_{b\ 0\ min}}\right)}$$

Animal housing

Male, adult Wistar rats were used for pharmacokinetic (Crl:WI(Han) [Charles River, Sulzfeld, Germany]) and pharmacology experiments (RccHan:WIST [Harlan, Horst, The Netherlands] or Crl:WI(Han)). All rats were maintained under standard lab conditions (temperature 20 ± 2°C, relative humidity 55–70%, standard Provimi Kliba diet 3336 [Kaiseraugst, Switzerland, www.kliba-nafag.ch], and domestic mains tap water *ad libitum*) on a regular 12-h light–dark cycle (lights on 06:00 AM). After arrival, rats were allowed at least one week of acclimatization to Actelion's animal facility and were carefully monitored to ensure good health and suitability for inclusion in the study. Unless noted otherwise, rats

were socially housed in groups of four in standard plastic rodent cages, and all tests were conducted during the light phase (08:00 AM to 6:00 PM) under illumination of >600 lx.

Pharmacokinetic experiments in the Beagle dog were performed in the Shanghai animal facilities of Actelion Pharmaceuticals Ltd in accordance with the Swiss animal protection law. The dogs were group-housed during the study and only separated for feeding and monitoring of clinical signs. With the exception of a period of fasting from the night before dose administration until 4 h after dose administration, animals were given a daily allowance of 350 g of a standard laboratory diet and had free access to tap water.

All animals were housed in accordance with the National Institute of Health guidelines and experimental procedures were approved by the Basel-Landschaft Veterinary Office and strictly adhered to Swiss federal regulations on animal experimentation. Well-being of animals was monitored during the day by trained technical stuff. Animals were checked on body weight loss, abnormal breathing, pilo-erection, grooming and locomotion as criteria of distress according to the company's animal welfare policy and guideline on humane endpoints.

Pharmacokinetic experiments in rat and dog

Male Wistar rats (n = 3) with a body weight of ca. 200–250 g were used for pharmacokinetic experiments under license no. 169. For intravenous sampling, a jugular vein catheter was implanted 2 days prior to drug dosing under aseptic conditions. After recovery from general isoflurane anesthesia, animals were housed individually with free access to water and food during the recovery period and the entire duration of the experiment. Compounds for intravenous use were formulated as aqueous solution in 30% 2-hydroxypropyl-beta-cyclodextrin (HPβCD) starting from a 5% stock solution in DMSO. For oral gavage dosing,

JPET Fast Forward. Published on June 29, 2017 as DOI: 10.1124/jpet.117.241596
This article has not been copyedited and formatted. The final version may differ from this version.

compounds were formulated as either a suspension in 0.5% methyl cellulose or as solution in PEG400.

Male Beagle dogs (n = 3) with body weights of 14.3–15.6 kg at the start of treatment were used in a cross-over design with a wash-out period of 7 days under license number 2016-06-QCB-32. All experiments were performed in fasted state, and gastric pH was controlled by giving intramuscular pentagastrin at a dose of 6 µg/kg 20 min before and 30 min after oral dosing. For intravenous dosing, compounds were formulated as aqueous solution in 30% HPβCD starting from a 5% stock solution in DMSO. For the oral route, compounds were either suspended in 0.5% methyl cellulose, dissolved in PEG400, or given as capsules containing either mannitol or a 4:1 mixture of Cremophor RH40 and lauroglycol.

Serial blood samples of 0.25 mL (rats) or 2 mL (dogs) were taken over a period of 24 h and transferred into vials fortified with EDTA as anticoagulant. Blood samples after oral dosing to rats were taken under light isoflurane anesthesia. Plasma was generated by centrifugation and stored at –20°C pending analysis.

Pharmacokinetic parameters were estimated using non-compartmental analysis within the Phoenix software package (version 6.4, Pharsight Corporation, Cary, USA). $AUC_{0\text{-}inf}$ was accepted if the percentage of area extrapolated to infinity ($AUC_{\%extp}$) did not exceed 20%, otherwise $AUC_{0\text{-}last}$ was reported.

Analytical methods

Samples from in vitro and in vivo experiments were fortified with 3–6 volume equivalents of methanol containing a close structural analog as internal standard, and proteins were removed by centrifugation at 3220 *g* for 20 min at 4°C. If required, supernatants were diluted with 1% aqueous formic acid or a 1:1 mixture of acetonitrile and 1% aqueous formic acid prior to quantification by liquid chromatography coupled to mass spectrometry (LC-MS/MS) on

API5000 or API5500 mass spectrometers (AB SCIEX, Concord, Ontario, Canada) in selected reaction monitoring mode. Chromatographic separation was achieved on Phenomenex Luna C8, C18, Gemini C18, Synergy Polar RP columns (4–5 μm, 2.0 × 20 mm ID) operated at room temperature with a flow rate of 0.6 mL/min, and using a linear gradient starting from 5–10% mobile phase B and a run time of 0.95 min. Mobile phases were 0.1% aqueous formic acid or 5 mM ammonium formate (pH 9, phase A) and acetonitrile or methanol (phase B).

Physiologically-based pharmacokinetic modeling

Simcyp® Population-Based absorption, distribution, metabolism, and excretion (ADME) Simulator (version 15; Sheffield, UK) was used for PBPK modeling and simulation PBPK models were built based on physicochemical, binding, permeability and metabolic stability data (**Table 7**). Oral absorption was modeled using the advanced dissolution, absorption, and metabolism (ADAM) model within Simcyp. Compounds were modeled as a solid formulation in immediate-release capsules for dog and human or as suspension for rat, using the diffusion-layer model of Wang and Flanagan (Jamei et al., 2009) to calculate the rate of dissolution from fine particles with an assumed diameter of 1 μm. The effect of bile salts upon dissolution and solubility was considered, matching the measured solubility in fasted state (FaSSIF) and fed state (FeSSIF) simulated intestinal fluids. Default values for particle density of 1.2 g/mL, a supersaturation ratio of 10, a precipitation rate constant of 15 min, and a diffusion layer thickness of 30 μm were assumed. A full PBPK, perfusion-limited distribution model was applied using method 2 within Simcyp, with an assumed tissue-to-plasma partition coefficient (K_p) scalar of 0.5 (Rodgers and Rowland, 2007; de Kanter et al., 2016). Elimination was assumed to be driven by CYP3A4-mediated metabolism, based on evidence for almorexant (Dingemanse et al., 2014), suvorexant (Cui et al., 2016), and ACT-541468 (AT, unpublished observation) using the well-stirred liver and ADAM gut model with $f_{u,gut}$ assumed to be 0.01. A factor of 2 was used to correct for the underprediction of *in*

JPET Fast Forward. Published on June 29, 2017 as DOI: 10.1124/jpet.117.241596
This article has not been copyedited and formatted. The final version may differ from this version.

vitro to *in vivo* CL. Thus, the model was populated with measured CL_{int} values from rat, dog or human liver microsomes, set to occur by hepatic and intestinal cyp3a (rat), cyp3a12 (dog) or CYP3A4 (human), multiplied by 2, and corrected for non-specific assay binding ($f_{u,mic}$, **Table 7**). OX_2 occupancy was estimated using predicted unbound brain concentration vs. time profiles, mean unbound K_b on the OX_2 receptor (**Table 1** and **Table 7**) and a sigmoid E_{max} model with an E_{max} of 100% and a Hill slope of 1.

$$\mathrm{OX_2\ occupancy} = \frac{E_{max}\ [\text{unbound brain concentration}]}{K_B + [\text{unbound brain concentration}]}$$

Free distribution of unbound drug between plasma and brain was assumed, as supported by the physico-chemical properties of all compounds and the absence of relevant P-gp and BCRP-mediated efflux (AT, unpublished observation).

Ten virtual trials of 10 subjects each were simulated in a male, healthy volunteer population with an age range of 18–45 years. Variation of all physiological parameters was based on the default variation in the healthy volunteer population database used in Simcyp.

Brain partitioning in the rat

Brain and plasma concentrations were determined 3 h following oral administration at 30 and 100 mg/kg to rats (n = 3–4 per group) under license no KV-BL-426. All compounds were formulated as solutions in PEG400. Blood was collected from the *vena cava caudalis* into plastic tubes containing EDTA as anticoagulant and centrifuged to yield plasma. Brain was collected after cardiac perfusion of 10 mL NaCl 0.9%. Brain tissue was then homogenized with one volume equivalent of cold phosphate buffer (pH 7.4), and compounds were extracted with methanol. Compound concentrations in plasma and brain were determined using LC-MS/MS as described above.

JPET Fast Forward. Published on June 29, 2017 as DOI: 10.1124/jpet.117.241596
This article has not been copyedited and formatted. The final version may differ from this version.

Telemetric sleep/wake cycle evaluation in rats

Sleep/wake cycles were evaluated based on electroencephalography/electromyography (EEG/EMG) and home cage activity recorded in individually housed Wistar rats under free-moving conditions under license no KV-BL-205. Rats (250-350 g, 6-8 weeks of age) were equipped with telemetric transmitters (TL11M2-F20-EET; Data Science International, St Paul, MN, USA) that allowed the noninvasive detection of EEG/EMG and activity via signal transmission to a receiver. The surgical transmitter implantation was performed under aseptic conditions. A pre-operative analgesia (buprenorphine 0.015 mg/kg s.c.) was administered 30 min before anesthesia. The entire surgical implantation was performed under general anesthesia (isoflurane inhalation [1–5% vol.] initiated in an anesthetic chamber). The rat was placed and secured in a stereotaxic apparatus. The body of the transmitter was placed subcutaneously along the dorsal flank of the rat with the leads routed subcutaneously to an incision accessing the cranium. For EEG recordings, two trepanations were placed in the skull, 2 mm from either side of the midline and 2 mm anterior to the lambda suture for placement of one differential pair of electrodes. Two other superficial trepanations were drilled for screws as support for cementing the electrodes. The EMG leads were inserted in either side of the muscles of the neck and sutured into place. After surgery, rats recovered from anesthesia in a chamber equipped with a heating pad at 37 ^{o}C. They were then housed individually and received analgesia with 0.015 mg/kg s.c. of buprenorphine b.i.d. for the first 2 days of the 2-week post-surgery recovery period. Before the experiment, rats were acclimatized for 3 days in their home cages placed in ventilated sound attenuating boxes, on a regular 12-h light/dark cycle. Experiments used a 'crossover' design, i.e., each animal was alternatively treated with a test compound and the vehicle, with at least 72 h between administrations. Treatments were administered orally (gavage) at the transition between the day and the night phase. Each telemetric recording covered a 24-h 'baseline' period preceding

the treatment, the 12-h night period immediately following the administration of treatment, and a 36-h recovery (wash-out) period. The recordings were split into a sequence of equal intervals of user-defined length (10 s). Sleep and wake stages (active wake, quiet wake, non-REM sleep, or REM sleep) were assigned to each interval automatically using the Somnologica Science software (Medcare, Embla, USA) based on frequency estimation for EEG, amplitude discrimination for the EMG, and the locomotor activity, as follows. Wake was characterized by low-amplitude EEG activity with relatively greater power in the higher frequency bands, such as alpha-band (10–13 Hz), accompanied by moderate to high levels of EMG activity. Active and quiet wake were distinguished based on the locomotor activity and the amplitude of the EMG. Non-REM sleep was defined by high-amplitude EEG activity with greater power in the delta frequency band (0.5–5 Hz) and low EMG activity. REM sleep was characterized by low-amplitude EEG activity focused in the theta frequency band (6–9 Hz) and no EMG activity. Data were analyzed by two-tailed paired Student's *t* test or one-way analysis of variance (ANOVA) followed by the post-hoc Tukey's multiple comparisons test, using GraphPad Prism (GraphPad Software). Differences were considered statistically significant at $p < 0.05$.

PK and PD assessments of ACT-541468 in healthy subjects

The single-dose pharmacokinetic profile of ACT-541468 after daytime and nighttime administration was assessed in the two single-center, double-blind, placebo-controlled, randomized studies AC-078-101 (NCT02919319) and AC-078-102 (NCT02571855). Both trials were conducted in full compliance with the principles of the Declaration of Helsinki, and study protocols were approved by independent Ethics Committees. Detailed information about study endpoints, inclusion and exclusion criteria are available at www.clinicaltrials.gov. For daytime pharmacokinetic assessments, 8 healthy male subjects received either placebo (n = 2) or ACT-541468 (n = 6) at doses of 5, 25, 50, 100, and 200

JPET Fast Forward. Published on June 29, 2017 as DOI: 10.1124/jpet.117.241596
This article has not been copyedited and formatted. The final version may differ from this version.

mg, given in the morning after overnight fasting. Blood samples were collected over a period of 96 h post-dose, plasma was separated by centrifugation, and ACT-541468 concentrations therein determined by LC-MS/MS. CL and V_{ss} were determined using an intravenous ^{14}C-ACT-541468 microdose given on top of 100 mg oral ACT-541468 (n=4). Plasma levels of radiolabeled ACT-541468 were quantified by accelerator mass spectrometry (AMS) technique after chromatographic separation. Pharmacokinetic parameters after nighttime administration were assessed in 6 healthy subjects who received either 25 mg ACT-541468 (n = 4) or placebo (n = 2). PD effects were assessed in study AC-078-101 at all doses after daytime administration of ACT-541468 during the first 10 h after dosing using a battery of objective tests including saccadic eye movements, adaptive tracking and body sway.

JPET Fast Forward. Published on June 29, 2017 as DOI: 10.1124/jpet.117.241596
This article has not been copyedited and formatted. The final version may differ from this version.

RESULTS

Inhibition of orexin receptor signaling in cellular assays

Almorexant and suvorexant have shown efficacy in inducing sleep in animals and humans, and, therefore, served as benchmark for the present benzimidazole series. **Table 1** and **Figure 2** summarize the characterization of the three benzimidazoles ACT-541468, ACT-605143 and ACT-658090 in calcium release assays in comparison with almorexant and suvorexant. The IC_{50} values measured at approximately EC_{70} of Ox_A (1.6 nM) were used to calculate the apparent K_b values. All five compounds behaved as potent dual antagonists, and displayed an insurmountable profile at both receptors. K_b values ranged from 0.52 to 8.3 nM at human OX_1 receptors, and from 0.42 nM to 5.9 nM at human OX_2 receptors. K_b values on the corresponding rat and human receptors were comparable (**Supplemental Table S1**). Using calcium release assays after antagonist wash-out, $ROt_{1/2}$ on OX_1 was estimated to be 6–9 min for suvorexant and all benzimidazoles, and 22 min for almorexant (**Table 2**). On OX_2, suvorexant, ACT-541468 and ACT-605143 showed $ROt_{1/2}$ in the range of 4–6 min, while $ROt_{1/2}$ was 13–14 min for ACT-658090 and almorexant. In summary, the three benzimidazoles displayed in vitro receptor interaction profiles similar to those of suvorexant and almorexant. ACT-541468 was a selective OX_1 and OX_2 receptor antagonist in a panel screen of more than 130 established central and peripheral pharmacological targets (AT, unpublished observation).

Pharmacology in the rat

Brain penetration

Brain penetration of ACT-541468, ACT-658090 and ACT-605143 was determined 3 h after administration of oral doses of 30 mg/kg and 100 mg/kg. At 30 mg/kg, mean total brain concentrations of ACT-541468 and ACT-658090 reached 665 nM and 614 nM but was only

JPET Fast Forward. Published on June 29, 2017 as DOI: 10.1124/jpet.117.241596
This article has not been copyedited and formatted. The final version may differ from this version.

154 nM for ACT-605143 (**Table 3**). Total brain levels increased in a more than dose-proportional manner at 100 mg/kg, reaching 2247–12,000 nM. Correction for *in vitro* brain binding ($f_{u,brain}$; **Table 7**) yielded unbound brain concentrations around or above the K_b values on rat OX_2 (**Supplemental Table S1**), warranting further investigations in a rat sleep model.

Effect on sleep/wake cycles in rats

All three benzimidazole DORAs were tested in male Wistar rats implanted with telemetric transmitters to allow for continuous EEG/EMG-based evaluation of sleep/wake cycles in freely moving animals in their home cages. ACT-541468, ACT-605143 and ACT-658090 were dosed at 30 mg/kg at the beginning of the night-active phase, when endogenous orexin levels are rising.

All three compounds showed robust effects on sleep/wake stages over the 6 h period post-dose (**Figure 3**). ACT-541468 decreased the time spent in active wake by 22% compared to vehicle-treated rats (–45 min; $p = 0.0068$, paired *t* test) and increased the time spent in non-REM and REM sleep by 29% and 84% (+26 and +10 min; $p = 0.0009$ and $p = 0.0228$), respectively. Latency to persistent non-REM sleep significantly decreased by 59% from 44 to 18 min ($p = 0.0002$), and to REM sleep by 58% from 71 to 30 min ($p = 0.0006$, **Figure 4**). A similar effect was observed with ACT-605143, which decreased the time spent in active wake by 21% compared to vehicle treated rats (–45 min; $p = 0.0089$), and increased the time spent in non-REM and REM sleep by 34% and 146% (+24 and +16 min; $p = 0.0092$ and $p < 0.001$), respectively. Latency to persistent non-REM sleep significantly decreased by 49% from 35 to 18 min ($p = 0.0033$, **Figure 4**), and to REM sleep by 44% from 62 to 35 min ($p = 0.007$). Finally, ACT-658090 decreased the time spent in active wake by 25% (–46 min; $p < 0.001$) and increased the time spent in quiet wake by 21% (+10 min; $p = 0.0099$). It increased the time spent in both non-REM and REM sleep by 27% and 57% (+26 min,

JPET Fast Forward. Published on June 29, 2017 as DOI: 10.1124/jpet.117.241596
This article has not been copyedited and formatted. The final version may differ from this version.

p = 0.0001; and +10 min, p = 0.0127), respectively. Latency to persistent non-REM sleep significantly decreased by 50% from 42 to 21 min (p = 0.030), and to REM sleep by 54% from 84 to 39 min (p = 0.032). Efficacy of the 3 benzimidazole DORAs over the 6 h period following a 30 mg/kg dose was similar (**Figure 4**). The increase in total sleep time over the 6 h period was between 36 and 40 min for all compounds and differences between compounds were not statistically significant (p = 0.9087, one-way ANOVA). Drug exposure, expressed as $AUC_{0\text{-last}}$, was also similar, within a 2.5-fold range from 2950–7510 nM·h (**Table 4**).

The dose response of ACT-541468 in the rat sleep model was characterized at 10, 30 and 100 mg/kg (**Figure 5**). ACT-541468 dose-dependently impacted sleep/wake parameters. Over the 6-h time period following administration, time spent in active wake decreased by 6 to 50 min, and time spent in non-REM and REM sleep increased by 2 to 29 min and 5 to 15 min, respectively. The lowest dose giving significant effects was 30 mg/kg. In the vehicle group, latency to persistent non-REM sleep varied from 40 to 47 min, depending on the group. Compared to vehicle, ACT-541468 significantly decreased the latency to persistent non-REM sleep to 18 min at 30 (p = 0.0002) or 100 mg/kg (p = 0.0079), and the latency to persistent REM sleep down to 30 min and 37 min at 30 mg/kg (p = 0.0006) and 100 mg/kg (p = 0.014), respectively.

In the vehicle-treated animals, the proportion of non-REM and REM sleep relative to total sleep time varied between 79–86% for non-REM sleep, and between 14–21% for REM sleep (**Table 5**). The proportion of non-REM and REM sleep did not change in a statistically significant manner for ACT-541468 at 30 mg/kg (p = 0.15) or 100 mg/kg (p = 0.59), or for ACT-658090 at 30 mg/kg (p = 0.27). In contrast, the time spent in non-REM sleep significantly decreased from 86% to 78% (p = 0.00074) for ACT-605143 at 30 mg/kg.

JPET Fast Forward. Published on June 29, 2017 as DOI: 10.1124/jpet.117.241596
This article has not been copyedited and formatted. The final version may differ from this version.

Pharmacokinetics in rat and dog

Pharmacokinetics of all 3 benzimidazole compounds were characterized in male rats and dogs in order to generate a database for validation of the respective PBPK models. Pharmacokinetic results after oral and intravenous administration are summarized in **Table 4** and **Table 6**, respectively. Plasma clearance (CL) of ACT-605143 and ACT-658090 in the rat was 32–36 mL/min/kg, and 85 mL/min/kg for ACT-541468. After correction for blood/plasma partitioning (**Table 7**), blood clearance of all three compounds was in a narrow range of 36–45 mL/min/kg, i.e., ca. 51–64% of liver blood flow in the rat. Plasma and blood clearances in the dog were 3.9–9.5 mL/min/kg and 6.5–15 mL/min/kg, respectively, the latter corresponding to 44–48% of liver blood flow for ACT-541468 and ACT-605143, but only 21% for ACT-658090. V_{ss} in the rat was in large excess of total body water, indicating significant drug distribution into tissues: 3.2 and 3.9 L/kg for ACT-541468 and ACT-658090, but only 0.8 L/kg for ACT-605143. V_{ss} in the dog was in a more narrow range, between 1.1–2.4 L/kg.

Oral absorption of all compounds was rapid in rat and dog, with peak plasma concentrations (C_{max}) being reached within 0.25–2.3 h (**Table 4**). Oral exposures ($AUC_{0\text{-last}}$) in the rat at 10 mg/kg varied by about 10-fold, from 412 nM·h for ACT-541468 to 4060 nM·h for ACT-658090, which was also reflected in their different oral bioavailability (F) of 9 vs. 43%. Smaller differences in $AUC_{0\text{-last}}$ were observed in the dog, with 2020 nM·h for ACT-541468 and 5610 nM·h for ACT-658090. Similar trends were evident for C_{max} in both species (**Table 4**).

PBPK model development for predicting human PK profiles

PBPK models for the benzimidazole DORAs ACT-541468, ACT-605143 and ACT-658090 were built based on *in silico* and biochemical data (**Table 7**), as outlined in **Figure 6**. PBPK models were initially developed for rat and dog and validated against observed PK data in

JPET Fast Forward. Published on June 29, 2017 as DOI: 10.1124/jpet.117.241596
This article has not been copyedited and formatted. The final version may differ from this version.

both species. All three PBPK models consistently overpredicted observed V_{ss}. Therefore, a K_p scalar of 0.5 was applied to empirically correct the predicted tissue-to-plasma ratios in all simulated tissues. In contrast, CL predictions underestimated observed values by approximately 2-fold, and microsomal CL_{int} was therefore multiplied by 2 in the PBPK models. The simulated pharmacokinetic parameters of these refined PBPK models after intravenous and oral dosing in rat and dog were considered similar enough to the observed values to construct the corresponding human PBPK models (**Table 4** and **Table 6)**. The simulated plasma concentration vs. time profiles and derived pharmacokinetic parameters of the three benzimidazoles in healthy volunteers at a dose of 25 mg are shown in **Figure 7A**. At this dose, the predicted fraction absorbed was 96–100% and not sensitive to the supersaturation ratio (1–100) or precipitation constant (0.4–40). Among the three compounds, ACT-541468 showed the fastest simulated oral absorption with a T_{max} of 2 h, the shortest initial half-life of 4.3 h, and the lowest C_{max} and $AUC_{0\text{-}24h}$ of 814 nM and 6500 nM·h, respectively (**Table 8**). ACT-658090 and ACT-605143 exhibited 5.9- to 7.3-fold higher $AUC_{0\text{-}24h}$, and 2.9–3.3 times higher C_{max}, and reached peak plasma concentrations later than ACT-541468, with T_{max} of 3.6–3.9 h. Most important for a sleep agent, plasma levels of ACT-658090 and ACT-605143 declined with relatively long half-lives of 10.4 and 26.8 h, resulting in significant residual drug levels at the end of the 24 h dosing interval (**Figure 7A**).

PBPK models for suvorexant and almorexant were developed using physicochemical and biochemical data (**Supplemental Table S2**) together with published clinical data for both compounds (Hoch et al., 2012; Sun et al., 2013; Dingemanse et al., 2014; TGA, 2014). For both, suvorexant and almorexant, oral absorption was modeled using ADAM and cellular permeability determined in MDCKII cells. Tissue distribution of suvorexant and almorexant was modeled as described above, while elimination was modeled based on published plasma clearances of 5 L/h and 43 L/h, respectively (Hoch et al., 2012; TGA, 2014). Final model

JPET Fast Forward. Published on June 29, 2017 as DOI: 10.1124/jpet.117.241596
This article has not been copyedited and formatted. The final version may differ from this version.

parameters after intravenous and oral dosing are presented in **Table 6** (CL and V_{ss}) and **Table 8** ($AUC_{0\text{-}24h}$, C_{max}, T_{max}, initial $T_{1/2}$)**.** The observed and simulated mean plasma concentration–time profiles of 40/50 mg suvorexant and 200 mg almorexant are shown in **Figure 8**.

Human dose estimates

PK/PD analysis of almorexant and suvorexant in rats as basis for human PD threshold concentrations

An attempt to estimate drug exposures needed to induce sleep in humans was done based on a PK/PD analysis in rats. The sleep-wake pattern in rats was analyzed after treatment with almorexant and suvorexant at doses of 10, 30 and 100 mg/kg given at the beginning of the active period (lights off), together with exposure data from PK experiments in a satellite group of rats. Both compounds were inactive at 10 mg/kg (**Supplemental Figure S2**), with almorexant and suvorexant plasma exposures in the first hours reaching 97 nM and 443 nM, respectively. At 30 mg/kg, total sleep time increased significantly with both compounds to about 3–7 h for almorexant, and about 2 h for suvorexant (**Supplemental Figure S2 and Figure S3**) at total and unbound plasma concentrations of ca. 195 nM and 1.2 nM for almorexant, and ca. 890 nM and 3.5 nM for suvorexant, which were regarded as PD threshold plasma concentrations in rat. Considering human plasma protein binding and the absence of potency differences at target receptors (**Table 1 and Supplemental Table S1)**, and assuming the need for similar degrees of OX_2 blockade in rats and humans, the predicted human PD threshold plasma concentrations would be 195 nM for almorexant and 3550 nM for suvorexant. These projected values were about 5- to 6-fold above the exposures observed in man with sleep-inducing doses of almorexant (200 mg; 8-h residual exposure of 20 ng/mL) and suvorexant (50 mg; 8-h residual exposure of 240 ng/mL; **Figure 8)**. It is noteworthy, that an exact determination of sleep duration in rats is technically difficult and is a methodological

limitation of this approach. Moreover, the fragmented sleep pattern in rats, i.e. alternating sleep and wake periods both in the active night and the inactive day period might render a direct translation of PD threshold concentrations from rat to humans difficult. Due to these uncertainties, human dose predictions were performed based on OX_2 receptor occupancy estimates.

Orexin 2 receptor occupancy estimates of almorexant and suvorexant in humans

Based on PBPK models of almorexant and suvorexant (**Table 8** and **Figure 8**) and assuming OX_2 blockade as the driving force for sleep maintenance, PBPK-PD models, i.e. OX_2 receptor occupancy vs. time profiles, were constructed using a sigmoid E_{max} model, unbound drug concentrations in brain, and the unbound K_b values for OX_2 inhibition shown in **Table 1**. OX_2 receptor occupancies were then estimated at 8 h post-dose as the presumed end of the sleep period (**Table 8**). According to these PBPK-PD models, 200 mg almorexant resulted in a peak OX_2 receptor occupancy of 81% at 2.5 h post-dose which declined to 63% at 8 h post-dose. Similarly, a 50 mg dose of suvorexant yielded a maximal OX_2 receptor occupancy of 73% reached at 3.2 h after drug intake which slowly declined to 66% at 8 h post-dose.

Human dose estimates for benzimidazole DORAs

The OX_2 receptor occupancy vs. time profiles of the three benzimidazole DORAs in healthy male subjects were derived starting from the respective PBPK models (**Figure 7A)**. OX_2 receptor occupancy vs. time profiles in brain (**Figure 7B)** were then predicted based on unbound brain concentrations, assuming that unbound drug in plasma readily equilibrates with brain and using the unbound K_b constants on OX_2 in a sigmoid E_{max} model with a Hill factor of 1. Using this approach, ACT-541468 doses were identified targeting an OX_2 receptor blockade of about 65% over a period of 8 h. As shown in **Table 8**, an ACT-541468

JPET Fast Forward. Published on June 29, 2017 as DOI: 10.1124/jpet.117.241596
This article has not been copyedited and formatted. The final version may differ from this version.

dose of 25 mg resulted in a predicted OX_2 receptor occupancy of 58% at 8 h post-dose. OX_2 receptor occupancies estimated for ACT-605143 and ACT-658090 at 8 h post-dose at the same 25 mg dose yielded values of 53% and 14%, respectively (**Table 8**).

ACT-541468 pharmacokinetics and pharmacodynamics in healthy subjects

The pharmacokinetic and pharmacodynamic profile of ACT-541468 was assessed in healthy subjects (n=6 on active, n= 2 on placebo) after daytime administration at doses ranging from 5-200 mg. Nighttime pharmacokinetic data were only generated for the 25 mg dose (n=4). Only data on the 25 mg dose are reported here. Geometric mean pharmacokinetic parameters (median for T_{max}) after daytime and nighttime are summarized in **Table 8** and are graphically depicted in **Figure 9**. After daytime administration, ACT-541468 was rapidly absorbed as judged from the median T_{max} of 1 h. Peak plasma concentrations and $AUC_{0\text{-}24h}$ were 1400 nM and 5700 nM·h, respectively. Oral absorption was slightly delayed to 1.5 h after nighttime dosing and peak plasma concentrations were reduced to 1050 nM. $AUC_{0\text{-}24h}$ was 8270 nM·h, i.e. about 45% higher compared to daytime administration. The pharmacodynamic effects of ACT-541468 were assessed during the first 10 h after dosing using a battery of objective tests including saccadic eye movements, adaptive tracking and body sway. The effect of 25 mg ACT-541468 on adaptive tracking as one of the most sensitive assessments of vigilance and attention is depicted in **Figure 10**.

CL and V_{ss} were determined from an intravenous ^{14}C-ACT-541468 microdose given on top of 100 mg oral ACT-541468 (n=4), followed by quantification of ACT-541468 using accelerator mass spectrometry (AMS) technique after chromatographic separation. Results are summarized in **Table 6** and were used for the validation of the human PBPK model.

JPET Fast Forward. Published on June 29, 2017 as DOI: 10.1124/jpet.117.241596
This article has not been copyedited and formatted. The final version may differ from this version.

DISCUSSION

An ideal sleep drug should mediate rapid sleep onset and sleep maintenance through major parts of the night and be devoid of next-day effects. While sleep onset may be optimized by appropriate formulation strategies including particle size control or use of solubility enhancers, sleep maintenance is dependent on intrinsic factors such as the time-course of target receptor blockade in the brain. Tools allowing for robust estimates of drug levels in human brain are therefore key for a successful sleep drug discovery program. Sleep models in rodent and non-rodent animal species have been conventionally used for this purpose and constitute an appropriate choice for compounds with little inter-species differences in receptor pharmacology and pharmacokinetics. Translation of animal data to man becomes challenging with prominent inter-species differences.

All three benzimidazole DORAs described here fulfill the basic requirements of a sleep drug. They are potent and insurmountable antagonists of both orexin receptors showing comparable K_b values on OX_1 and OX_2 (**Table 1**). In line with their physico-chemical properties and the absence of relevant P-gp efflux, they readily cross the blood-brain barrier, as evidenced by the similarity of unbound brain and plasma concentrations in rats (**Table 3**). A 30 mg/kg dose increased non-REM, REM, and total sleep time in telemetrized rats, and decreased the latency to the first episode of persistent non-REM and REM sleep compared to vehicle-treated animals. The pharmacological profiles in the rat were similar to each other and comparable to other DORAs described in literature (Aissaoui et al., 2008; Boss et al., 2008; Cox et al., 2010; Sifferlen et al., 2010; Winrow et al., 2012; Sifferlen et al., 2013; Boss et al., 2014; Sifferlen et al., 2015; Heidmann et al., 2016). No clear differentiation between compounds was therefore possible on the basis of drug efficacy in rats.

JPET Fast Forward. Published on June 29, 2017 as DOI: 10.1124/jpet.117.241596
This article has not been copyedited and formatted. The final version may differ from this version.

In contrast, the benzimidazoles exhibited significant inter-species differences in key parameters driving drug distribution and clearance (**Table 7**). Metabolic stability in liver microsomes differed by 7.2- to 14-fold between rat and human, while plasma protein binding, the major determinant for general tissue and specifically brain penetration, differed by 9- to 30-fold. Ratios of unbound brain and plasma concentrations in the rat were below unity and increased with dose **(Table 3)**. Non-linear plasma protein binding was demonstrated for ACT-541468 at concentrations relevant for rat pharmacology assessments but not clinical testing (**Supplemental Table S3**), which might, at least in part, contribute to the dose-dependent brain/plasma ratios. Other factors, such as P-gp or bcrp-mediated efflux might also play a role in rats but have been excluded for man. Pharmacokinetic behavior was therefore expected to significantly differ between rat and man, calling for a tailored approach for the identification of a candidate drug exhibiting, beyond rapid sleep onset and efficacy, a sleep maintenance in man not longer than 8 h.

The pharmacokinetic differences predicted for these benzimidazoles are mostly a reflection of differences in drug CL and tissue distribution (**Table 6** and **Figure 7A**). ACT-541468 had a 6–12 times higher simulated CL compared to ACT-605143 and ACT-658090 (**Table 6**), resulting from its intrinsic clearance (CL_{int}) in liver microsomes and the lowest binding to plasma and liver microsomal proteins (**Table 7**). On the other hand, ACT-541468 exhibited a larger simulated volume of distribution, i.e. 0.5 L/kg vs. 0.2 L/kg, in line with its lower plasma protein binding and distribution coefficient (logD). The combination of higher clearance and larger volume of distribution resulted in a simulated initial ACT-541468 plasma half-life of only 4.3 h, which favorably compared to the 10.4 h and 26.8 h of ACT-605143 or ACT-658090, respectively, and also to suvorexant with a simulated half-life of 8.7 h. It is noteworthy, that these differences in pharmacokinetic profiles were not obvious from

JPET Fast Forward. Published on June 29, 2017 as DOI: 10.1124/jpet.117.241596
This article has not been copyedited and formatted. The final version may differ from this version.

simple inspection of the individual modeling input data such as CL_{int}, plasma or microsomal binding, pK_a and logD, which were all within a 2- to 3-fold range.

Published data on human pharmacodynamics and pharmacokinetics of 200 mg almorexant (Hoever et al., 2012a) and 50 mg suvorexant (Sun et al., 2013) after nighttime administration were used as a basis to estimate active doses of the benzimidazoles in man. Initial inspection of the plasma concentration vs. time profiles of both compounds at the end of the presumed 8-h sleep period indicated residual almorexant and suvorexant plasma concentrations of 20 ng/mL and 240 ng/mL, respectively (**Figure 8**). This 12-fold difference in total plasma concentrations between both compounds appeared somewhat surprising in light of apparently identical OX_2 receptor potency in cellular assays (**Table 1**). Introducing corrections for molecular weight, plasma protein binding, and non-specific binding in the orexin binding assays (**Table 7**) yielded comparable unbound almorexant and suvorexant concentrations of 1.5 and 2.3, when expressed as multiples of their respective unbound K_b values at OX_2. PBPK-PD models constructed for both antagonists yielded consistent levels of OX_2 receptor occupancy of 63–66% at the end of an 8-h period (**Table 8**). A very similar threshold of 65–80% was recently reported for other DORAs in rat and dog (Gotter et al., 2013). While almorexant and suvorexant both exhibited the same degree of OX_2 receptor blockade at 8 h post-dose, only suvorexant was associated with impaired next-day performance (Citrome, 2014; Vermeeren et al., 2015). In addition to the absolute values in OX_2 blockade, their rate of decline at the end of the sleep period was identified as a second key factor determining the absence of next day effects. The 65% OX_2 threshold was then used as guidance for predicting active doses of the benzimidazoles (**Figure 7B**). The time course of OX_2 receptor blockade generally followed plasma concentrations for all three compounds. Major differences were, however, observed in the magnitude of OX_2 blockade. Despite the lowest simulated total plasma exposure, ACT-541468 elicited the highest peak OX_2 receptor blockade of 79%,

JPET Fast Forward. Published on June 29, 2017 as DOI: 10.1124/jpet.117.241596
This article has not been copyedited and formatted. The final version may differ from this version.

while only 59% were reached with ACT-605143. Differences in plasma protein binding compensated for the 2.9-fold higher total plasma concentrations of ACT-605143, resulting in almost equal unbound peak concentrations of ACT-541468 in brain, i.e., 1.1 nM vs. 0.96 nM. At 8 h post-dose, OX_2 receptor occupancies were 58% for ACT-541468 and 53% for ACT-605143, indicating that both compounds met the requirement to maintain sleep over an 8-h period. Slightly lower OX_2 receptor occupancies than those deduced from clinical data on almorexant and suvorexant were targeted on purpose to compensate for the higher drug concentrations expected after nighttime dosing (Hoever et al., 2012a; Sun et al., 2013), which PBPK-PD modeling was technically unable to capture. Compared to ACT-605143, the decline in OX_2 receptor occupancy was faster with ACT-541468, in line with the higher CL, lower V_{ss} and resulting shorter half-life (**Table 6**). Based on PBPK-PD modeling, ACT-658090 was predicted to elicit a maximum OX_2 receptor blockade of only 15%. This somewhat surprising outcome in light of the excellent pharmacokinetic profile **(Figure 7A)** is best explained by the lower OX_2 receptor potency combined with very high plasma binding (**Table 7**), resulting in insufficient unbound drug levels in brain to elicit relevant OX_2 receptor blockade. Based on above analysis and its overall favorable profile in terms of animal pharmacology, early safety and drug-drug interaction potential (AT, unpublished observation), ACT-541468 was selected for clinical development.

The pharmacokinetic profile of ACT-541468 in healthy subjects was characterized after daytime and nighttime administration in two Phase 1 studies, while its pharmacodynamics were assessed during the first 10 h after daytime administration using a battery of objective and subjective assessments. Observed PK parameters at a dose of 25 mg, (**Table 8** and **Figure 9**), indicated rapid oral absorption after daytime administration with peak plasma concentrations of 1400 nM being reached within 1 h. Plasma $AUC_{0\text{-}24h}$ was well predicted within a 14% range. The observed initial half-life was 3.0 h and thus slightly shorter than the

simulated value of 4.3 h, well in accordance with the higher observed CL, i.e., 1.0 mL/min/kg vs. predicted 1.2 mL/min/kg, and lower V_{ss}, 0.4 L/kg vs. 0.5 L/kg (**Table 6**). The terminal half-life of ACT-541468 was about 6 h (Mühlan et al., 2017). After nighttime dosing of ACT-541468, mean peak plasma concentrations only reached 1050 nM while $AUC_{0\text{-}24h}$ increased by 27% to 8270 nM·h. Oral absorption was slightly delayed, with a T_{max} of 1.5 h, and plasma half-life increased from 3.0 h to 5.1 h. The differences between ACT-541468 daytime and nighttime pharmacokinetics may result from diurnal differences in physiology between night and day such as intestinal motility and perfusion, or liver blood flow. It is important to note, that the observed differences in ACT-541468 PK were rather small, in contrast to the significantly delayed oral absorption and reduced plasma levels after nighttime administration of almorexant (**Table 8** and **Figure 8)** (Hoever et al., 2012a). From a methodological point of view it is noteworthy, that PK simulations were run with a total of 100 subjects, while the observed PK data are means of only six and four healthy subjects, which might not properly represent a larger population. Pharmacodynamically, 25 mg ACT-541468 revealed significantly reduced vigilance and attention (**Figure 10**), and had clear effects on visuomotor coordination and postural stability. Onset of effects was observed within 1 h, and returned to baseline within 3–6 h. These early assessments in healthy subjects after daytime dosing suggest that a 25 mg dose has the potential to elicit the desired sleep effects in insomnia patients.

In conclusion, we describe the discovery of the dual orexin receptor antagonist ACT-541468 based on early use of PBPK and PD modeling as part of the lead optimization process. ACT-541468 was identified out of a larger set of structurally related derivatives based on its simulated OX_2 receptor occupancy, targeting for an effect duration of about 8 h at a 25 mg dose, and a sufficiently short half-life to minimize next-day effects. Phase I clinical trials with ACT-541468 in healthy subjects confirmed PBPK model-based predictions, as ACT-541468

JPET Fast Forward. Published on June 29, 2017 as DOI: 10.1124/jpet.117.241596
This article has not been copyedited and formatted. The final version may differ from this version.

reached peak plasma concentrations within 1 h after dosing and exhibited an initial plasma half-life of only 3 h. Drug exposure at a dose of 25 mg reduced vigilance and attention, and impaired visuomotor coordination and postural stability in healthy subjects after daytime administration. Differences between nighttime and daytime PK performance may result from diurnal changes in physiology but are not expected to negatively impact on performance of ACT-541468 in insomnia patients.

JPET Fast Forward. Published on June 29, 2017 as DOI: 10.1124/jpet.117.241596
This article has not been copyedited and formatted. The final version may differ from this version.

ACKNOWLEDGMENTS

The authors would like to thank Stephane Delahaye, Susanne Globig, Bruno Capeleto, Charlyse Herrmann, Pascal Rebmann, Daniela Kruesi, Marc Candreia, Ursula Fusco-Hug, Thomas Sasse, Katalin Menyhart, Celia Müller, Cédric Fischer, Hélène Massinet and Hélène Roellinger for their dedication and expert experimental contributions. The authors would like to thank Alexey Veligodskiy for his help in the writing of the manuscript.

AUTHORSHIP CONTRIBUTIONS

Participated in research design: *A.T., R.d.K., C.R., J.G., C.B., M.v.R., C.M.*

Conducted experiments: *A.T., R.d.K., C.R., J.G., C.B., M.v.R., C.M., J.v.G.*

Performed data analysis: *A.T., R.d.K., C.R., J.G., C.B., M.v.R, C.M.*

Wrote or contributed to the writing of the manuscript: *A.T., R.d.K., C.R., J.G., C.B., B.S., F.J.*

All experiments described in this report have been conducted in the research facilities of Actelion Pharmaceuticals Ltd. During manuscript preparation and review, Actelion Pharmaceuticals Ltd was acquired by Johnson & Johnson, and its drug discovery and early development activities subsequently transferred into a newly created company, Idorsia Pharmaceuticals Ltd. With the exception of Joop van Gerven, all authors of this report were employees of Idorsia Pharmaceuticals Ltd at the time of manuscript publication.

REFERENCES

Aissaoui H, Koberstein R, Zumbrunn C, Gatfield J, Brisbare-Roch C, Jenck F, Treiber A and Boss C (2008) N-Glycine-sulfonamides as potent dual orexin 1/orexin 2 receptor antagonists. *Bioorganic & medicinal chemistry letters* **18**:5729-5733.

Baxter CA, Cleator E, Brands KMJ, Edwards JS, Reamer RA, Sheen FJ, Stewart GW, Strotman NA and Wallace DJ (2011) The first large-scale synthesis of MK-4305: a dual orexin receptor antagonist for the treatment of sleep disorder. *Organic Process Research & Development* **15**:367-375.

Bettica P, Nucci G, Pyke C, Squassante L, Zamuner S, Ratti E, Gomeni R and Alexander R (2012a) Phase I studies on the safety, tolerability, pharmacokinetics and pharmacodynamics of SB-649868, a novel dual orexin receptor antagonist. *J Psychopharmacol* **26**:1058-1070.

Bettica P, Squassante L, Groeger JA, Gennery B, Winsky-Sommerer R and Dijk DJ (2012b) Differential effects of a dual orexin receptor antagonist (SB-649868) and zolpidem on sleep initiation and consolidation, SWS, REM sleep, and EEG power spectra in a model of situational insomnia. *Neuropsychopharmacology* **37**:1224-1233.

Bonaventure P, Shelton J, Yun S, Nepomuceno D, Sutton S, Aluisio L, Fraser I, Lord B, Shoblock J, Welty N, Chaplan SR, Aguilar Z, Halter R, Ndifor A, Koudriakova T, Rizzolio M, Letavic M, Carruthers NI, Lovenberg T and Dugovic C (2015a) Characterization of JNJ-42847922, a selective orexin-2 receptor antagonist, as a clinical candidate for the treatment of insomnia. *J Pharmacol Exp Ther* **354**:471-482.

Bonaventure P, Yun S, Johnson PL, Shekhar A, Fitz SD, Shireman BT, Lebold TP, Nepomuceno D, Lord B, Wennerholm M, Shelton J, Carruthers N, Lovenberg T and Dugovic C (2015b) A selective orexin-1 receptor antagonist attenuates stress-induced hyperarousal without hypnotic effects. *J Pharmacol Exp Ther* **352**:590-601.

Boss C, Brisbare-Roch C, Jenck F, Aissaoui H, Koberstein R, Sifferlen T and Weller T (2008) Orexin receptor antagonism: a new principle in neuroscience. *Chimia* **62**:974-979.

Boss C, Brotschi C, Gude M, Heidmann B, Sifferlen T, Von Raumer M and Williams JT (2015a) Published Patent Application WO/2015/083070. Crystalline form of (s)-(2-(6-chloro-7-methyl-1h-benzo[d]imidazol-2-yl)-2-methylpyrrolidin-1-yl)(5-methoxy-2-(2H-1,2,3-triazol-2-yl)phenyl)methanone and its use as orexin receptor antagonists. Application number PCT/IB2014/066508. Filed on 02.12.2014; published on 11.06.2015.

Boss C, Brotschi C, Gude M, Heidmann B, Sifferlen T and Williams JT (2013) Published Patent Application WO/2013/182972. Benzimidazole-proline derivatives. Application number PCT/IB2013/054567. Filed on 03.06.2013; published on 12.12.2013.

Boss C, Roch-Brisbare C, Steiner MA, Treiber A, Dietrich H, Jenck F, von Raumer M, Sifferlen T, Brotschi C, Heidmann B, Williams JT, Aissaoui H, Siegrist R and Gatfield J (2014) Structure-activity relationship, biological, and pharmacological characterization of the proline sulfonamide ACT-462206: a potent, brain-penetrant dual orexin 1/orexin 2 receptor antagonist. *ChemMedChem* **9**:2486-2496.

Boss C, Roch C, Brotschi C, Gude M, Heidmann B, Jenck F, Sifferlen T, Steiner MA and Williams JT (2015b) Published Patent Application WO/2015/083094. Use of benzimidazole-proline derivatives. Application number PCT/IB2014/066548. Filed on 03.12.2014; published on 11.06.2015.

Carter ME, Borg JS and de Lecea L (2009) The brain hypocretins and their receptors: mediators of allostatic arousal. *Curr Opin Pharmacol* **9**:39-45.

Cheng Y and Prusoff WH (1973) Relationship between the inhibition constant (Ki) and the concentration of inhibitor which causes 50 per cent inhibition (IC_{50}) of an enzymatic reaction. *Biochem Pharmacol* **22**:3099-3108.

Chung JY, Zhong YL, Maloney KM, Reamer RA, Moore JC, Strotman H, Kalinin A, Feng R, Strotman NA, Xiang B and Yasuda N (2014) Unusual pyrimidine participation: efficient stereoselective synthesis of potent dual orexin receptor antagonist MK-6096. *Org Lett* **16**:5890-5893.

Citrome L (2014) Suvorexant for insomnia: a systematic review of the efficacy and safety profile for this newly approved hypnotic - what is the number needed to treat, number needed to harm and likelihood to be helped or harmed? *Int J Clin Pract* **68**:1429-1441.

Connor KM, Mahoney E, Jackson S, Hutzelmann J, Zhao X, Jia N, Snyder E, Snavely D, Michelson D, Roth T and Herring WJ (2016) A phase II dose-ranging study evaluating the efficacy and safety of the orexin receptor antagonist filorexant (MK-6096) in patients with primary insomnia. *Int J Neuropsychopharmacol* doi: 10.1093/ijnp/pyw022.

Cox CD, Breslin MJ, Whitman DB, Schreier JD, McGaughey GB, Bogusky MJ, Roecker AJ, Mercer SP, Bednar RA, Lemaire W, Bruno JG, Reiss DR, Harrell CM, Murphy KL, Garson SL, Doran SM, Prueksaritanont T, Anderson WB, Tang C, Roller S, Cabalu TD, Cui D, Hartman GD, Young SD, Koblan KS, Winrow CJ, Renger JJ and Coleman PJ (2010) Discovery of the dual orexin receptor antagonist [(7R)-4-(5-chloro-1,3-benzoxazol-2-yl)-7-methyl-1,4-diazepan-1-yl][5-methyl-2-(2H-1,2,3-triazol-2-yl)phenyl]methanone (MK-4305) for the treatment of insomnia. *J Med Chem* **53**:5320-5332.

Cui D, Cabalu T, Yee KL, Small J, Li X, Liu B, Maciolek C, Smith S, Liu W, McCrea JB and Prueksaritanont T (2016) In vitro and in vivo characterisation of the metabolism and disposition of suvorexant in humans. *Xenobiotica* **46**:882-895.

de Kanter R, Sidharta PN, Delahaye S, Gnerre C, Segrestaa J, Buchmann S, Kohl C and Treiber A (2016) Physiologically-based pharmacokinetic modeling of macitentan: prediction of drug-drug interactions. *Clin Pharmacokinet* **55**:369-380.

de Lecea L, Kilduff TS, Peyron C, Gao X, Foye PE, Danielson PE, Fukuhara C, Battenberg EL, Gautvik VT, Bartlett FS, 2nd, Frankel WN, van den Pol AN, Bloom FE, Gautvik KM and Sutcliffe JG (1998) The hypocretins: hypothalamus-specific peptides with neuroexcitatory activity. *Proc Natl Acad Sci U S A* **95**:322-327.

Dingemanse J, Cruz HG, Gehin M and Hoever P (2014) Pharmacokinetic interactions between the orexin receptor antagonist almorexant and the CYP3A4 inhibitors ketoconazole and diltiazem. *J Pharm Sci* **103**:1548-1556.

Dugovic C, Shelton JE, Yun S, Bonaventure P, Shireman BT and Lovenberg TW (2014) Orexin-1 receptor blockade dysregulates REM sleep in the presence of orexin-2 receptor antagonism. *Front Neurosci* doi: 10.3389/fnins.2014.00028.

Frey DJ, Ortega JD, Wiseman C, Farley CT and Wright KP, Jr. (2011) Influence of zolpidem and sleep inertia on balance and cognition during nighttime awakening: a randomized placebo-controlled trial. *J Am Geriatr Soc* **59**:73-81.

Girardin M, Ouellet SG, Gauvreau D, Moore JC, Hughes G, Devine PN, O'Shea PD and Campeau L-C (2013) Convergent kilogram-scale synthesis of dual orexin receptor antagonist. *Organic Process Research & Development* **17**:61-68.

Glass J, Lanctot KL, Herrmann N, Sproule BA and Busto UE (2005) Sedative hypnotics in older people with insomnia: meta-analysis of risks and benefits. *BMJ* doi: 10.1136/bmj.38623.768588.47.

Gotter AL, Forman MS, Harrell CM, Stevens J, Svetnik V, Yee KL, Li X, Roecker AJ, Fox SV, Tannenbaum PL, Garson SL, Lepeleire ID, Calder N, Rosen L, Struyk A, Coleman PJ, Herring WJ, Renger JJ and Winrow CJ (2016) Orexin 2 receptor antagonism is sufficient to promote NREM and REM sleep from mouse to man. *Sci Rep* doi: 10.1038/srep27147.

Gotter AL, Winrow CJ, Brunner J, Garson SL, Fox SV, Binns J, Harrell CM, Cui D, Yee KL, Stiteler M, Stevens J, Savitz A, Tannenbaum PL, Tye SJ, McDonald T, Yao L, Kuduk SD, Uslaner J, Coleman PJ and Renger JJ (2013) The duration of sleep promoting efficacy by dual orexin receptor antagonists is dependent upon receptor occupancy threshold. *BMC Neurosci* doi: 10.1186/1471-2202-14-90.

Gozzi A, Turrini G, Piccoli L, Massagrande M, Amantini D, Antolini M, Martinelli P, Cesari N, Montanari D, Tessari M, Corsi M and Bifone A (2011) Functional magnetic resonance imaging reveals different neural substrates for the effects of orexin-1 and orexin-2 receptor antagonists. *PLoS One* **6**:e16406.

Heidmann B, Gatfield J, Roch C, Treiber A, Tortoioli S, Brotschi C, Williams JT, Bolli MH, Abele S, Sifferlen T, Jenck F and Boss C (2016) Discovery of highly potent dual orexin receptor antagonists via a scaffold-hopping approach. *ChemMedChem* doi: 10.1002/cmdc.201600175.

Herring WJ, Snyder E, Budd K, Hutzelmann J, Snavely D, Liu K, Lines C, Roth T and Michelson D (2012) Orexin receptor antagonism for treatment of insomnia: a randomized clinical trial of suvorexant. *Neurology* **79**:2265-2274.

Hoch M, Hoever P, Zisowsky J, Priestley A, Fleet D and Dingemanse J (2012) Absolute oral bioavailability of almorexant, a dual orexin receptor antagonist, in healthy human subjects. *Pharmacology* **89**:53-57.

Hoever P, de Haas SL, Dorffner G, Chiossi E, van Gerven JM and Dingemanse J (2012a) Orexin receptor antagonism: an ascending multiple-dose study with almorexant. *J Psychopharmacol* **26**:1071-1080.

Hoever P, Dorffner G, Benes H, Penzel T, Danker-Hopfe H, Barbanoj MJ, Pillar G, Saletu B, Polo O, Kunz D, Zeitlhofer J, Berg S, Partinen M, Bassetti CL, Hogl B, Ebrahim IO, Holsboer-Trachsler E, Bengtsson H, Peker Y, Hemmeter UM, Chiossi E, Hajak G and

Dingemanse J (2012b) Orexin receptor antagonism, a new sleep-enabling paradigm: a proof-of-concept clinical trial. *Clin Pharmacol Ther* **91**:975-985.

Jacobson LH, Chen S, Mir S and Hoyer D (2016) Orexin OX2 receptor antagonists as sleep aids. *Curr Top Behav Neurosci* doi: 10.1007/7854_2016_47.

Jamei M, Turner D, Yang J, Neuhoff S, Polak S, Rostami-Hodjegan A and Tucker G (2009) Population-based mechanistic prediction of oral drug absorption. *AAPS J* **11**:225-237.

Johnson PL, Samuels BC, Fitz SD, Lightman SL, Lowry CA and Shekhar A (2012) Activation of the orexin 1 receptor is a critical component of CO_2-mediated anxiety and hypertension but not bradycardia. *Neuropsychopharmacology* **37**:1911-1922.

Jones HM, Gardner IB and Watson KJ (2009) Modelling and PBPK simulation in drug discovery. *AAPS J* **11**:155-166.

Kochansky CJ, McMasters DR, Lu P, Koeplinger KA, Kerr HH, Shou M and Korzekwa KR (2008) Impact of pH on plasma protein binding in equilibrium dialysis. *Mol Pharm* **5**:438-448.

Mahler SV, Moorman DE, Smith RJ, James MH and Aston-Jones G (2014) Motivational activation: a unifying hypothesis of orexin/hypocretin function. *Nat Neurosci* **17**:1298-1303.

Mangion IK, Sherry BD, Yin J and Fleitz FJ (2012) Enantioselective synthesis of a dual orexin receptor antagonist. *Org Lett* **14**:3458-3461.

Merlo Pich E and Melotto S (2014) Orexin 1 receptor antagonists in compulsive behavior and anxiety: possible therapeutic use. *Front Neurosci* doi: 10.3389/fnins.2014.00026.

Mieda M, Hasegawa E, Kisanuki YY, Sinton CM, Yanagisawa M and Sakurai T (2011) Differential roles of orexin receptor-1 and -2 in the regulation of non-REM and REM sleep. *J Neurosci* **31**:6518-6526.

Miller TR, Witte DG, Ireland LM, Kang CH, Roch JM, Masters JN, Esbenshade TA and Hancock AA (1999) Analysis of apparent noncompetitive responses to competitive H(1)-histamine receptor antagonists in fluorescent imaging plate reader-based calcium assays. *J Biomol Screen* **4**:249-258.

Mühlan C, Juif PE, Van Gerven J, Heuberger J and Dingemanse J (2017) First-in-man study of ACT-541468, a novel dual orexin receptor antagonist: characterization of its pharmacokinetics, pharmacodynamics, safety and tolerability. In: American Society for Clinical Pharmacology and Therapeutics 2017 Annual Meeting Abstracts. *Clin Pharmacol Ther* **101**:S5–S99.

Obach RS and Reed-Hagen AE (2002) Measurement of Michaelis constants for cytochrome P450-mediated biotransformation reactions using a substrate depletion approach. *Drug Metab Dispos* **30**:831-837.

Otmani S, Demazieres A, Staner C, Jacob N, Nir T, Zisapel N and Staner L (2008) Effects of prolonged-release melatonin, zolpidem, and their combination on psychomotor functions, memory recall, and driving skills in healthy middle aged and elderly volunteers. *Hum Psychopharmacol* **23**:693-705.

Peyron C, Faraco J, Rogers W, Ripley B, Overeem S, Charnay Y, Nevsimalova S, Aldrich M, Reynolds D, Albin R, Li R, Hungs M, Pedrazzoli M, Padigaru M, Kucherlapati M, Fan J, Maki R, Lammers GJ, Bouras C, Kucherlapati R, Nishino S and Mignot E (2000) A mutation in a case of early onset narcolepsy and a generalized absence of hypocretin peptides in human narcoleptic brains. *Nat Med* **6**:991-997.

Ramirez AD, Gotter AL, Fox SV, Tannenbaum PL, Yao L, Tye SJ, McDonald T, Brunner J, Garson SL, Reiss DR, Kuduk SD, Coleman PJ, Uslaner JM, Hodgson R, Browne SE, Renger JJ and Winrow CJ (2013) Dual orexin receptor antagonists show distinct effects on locomotor performance, ethanol interaction and sleep architecture relative to gamma-

aminobutyric acid-A receptor modulators. *Front Neurosci* doi: 10.3389/fnins.2013.00254.

Rodgers T and Rowland M (2007) Mechanistic approaches to volume of distribution predictions: understanding the processes. *Pharm Res* **24**:918-933.

Sakurai T (1999) Orexins and orexin receptors: implication in feeding behavior. *Regul Pept* **85**:25-30.

Sakurai T (2007) The neural circuit of orexin (hypocretin): maintaining sleep and wakefulness. *Nat Rev Neurosci* **8**:171-181.

Sifferlen T, Boller A, Chardonneau A, Cottreel E, Gatfield J, Treiber A, Roch C, Jenck F, Aissaoui H, Williams JT, Brotschi C, Heidmann B, Siegrist R and Boss C (2015) Substituted pyrrolidin-2-ones: Centrally acting orexin receptor antagonists promoting sleep. Part 2. *Bioorganic & medicinal chemistry letters* **25**:1884-1891.

Sifferlen T, Boss C, Cottreel E, Koberstein R, Gude M, Aissaoui H, Weller T, Gatfield J, Brisbare-Roch C and Jenck F (2010) Novel pyrazolo-tetrahydropyridines as potent orexin receptor antagonists. *Bioorganic & medicinal chemistry letters* **20**:1539-1542.

Sifferlen T, Koberstein R, Cottreel E, Boller A, Weller T, Gatfield J, Brisbare-Roch C, Jenck F and Boss C (2013) Synthesis, structure-activity relationship studies, and identification of novel 5,6,7,8-tetrahydroimidazo[1,5-a]pyrazine derivatives as dual orexin receptor antagonists. Part 1. *Bioorganic & medicinal chemistry letters* **23**:2212-2216.

Sun H, Kennedy WP, Wilbraham D, Lewis N, Calder N, Li X, Ma J, Yee KL, Ermlich S, Mangin E, Lines C, Rosen L, Chodakewitz J and Murphy GM (2013) Effects of suvorexant, an orexin receptor antagonist, on sleep parameters as measured by polysomnography in healthy men. *Sleep* **36**:259-267.

Sun H, Yee KL, Gill S, Liu W, Li X, Panebianco D, Mangin E, Morrison D, McCrea J, Wagner JA and Troyer MD (2015) Psychomotor effects, pharmacokinetics and safety of

the orexin receptor antagonist suvorexant administered in combination with alcohol in healthy subjects. *J Psychopharmacol* **29**:1159-1169.

Tannenbaum PL, Tye SJ, Stevens J, Gotter AL, Fox SV, Savitz AT, Coleman PJ, Uslaner JM, Kuduk SD, Hargreaves R, Winrow CJ and Renger JJ (2016) Inhibition of orexin signaling promotes sleep yet preserves salient arousability in monkeys. *Sleep* **39**:603-612.

TGA (2014) Australian Government, Department of Health, Therapeutic Goods Administration. Australian Public Assessment Report Attachment 1: Extract from the clinical evaluation report for suvorexant. Available at: www.tga.gov.au/sites/default/files/auspar-suvorexant-150411-cer.pdf. Accessed on: 11 November 2016.

Thannickal TC, Moore RY, Nienhuis R, Ramanathan L, Gulyani S, Aldrich M, Cornford M and Siegel JM (2000) Reduced number of hypocretin neurons in human narcolepsy. *Neuron* **27**:469-474.

Tsujino N and Sakurai T (2009) Orexin/Hypocretin: a neuropeptide at the interface of sleep, energy homeostasis, and reward system. *Pharmacol Rev* **61**:162-176.

Vermeeren A, Sun H, Vuurman EF, Jongen S, Van Leeuwen CJ, Van Oers AC, Palcza J, Li X, Laethem T, Heirman I, Bautmans A, Troyer MD, Wrishko R and McCrea J (2015) On-the-road driving performance the morning after bedtime use of suvorexant 20 and 40 mg: a study in non-elderly healthy volunteers. *Sleep* **38**:1803-1813.

Verzijl GKM, de Vries AHM, de Vries JG, Kapitan P, Dax T, Helms M, Nazir Z, Skranc W, Imboden C, Stichler J, Ward RA, Abele S and Lefort L (2013) Catalytic asymmetric reduction of a 3,4-dihydroisoquinoline for the large-scale production of almorexant: hydrogenation or transfer hydrogenation? *Organic Process Research & Development* **17**:1531-1539.

Wan H and Rehngren M (2006) High-throughput screening of protein binding by equilibrium dialysis combined with liquid chromatography and mass spectrometry. *J Chromatogr A* **1102**:125-134.

Waters NJ, Jones R, Williams G and Sohal B (2008) Validation of a rapid equilibrium dialysis approach for the measurement of plasma protein binding. *J Pharm Sci* **97**:4586-4595.

Winrow CJ, Gotter AL, Cox CD, Tannenbaum PL, Garson SL, Doran SM, Breslin MJ, Schreier JD, Fox SV, Harrell CM, Stevens J, Reiss DR, Cui D, Coleman PJ and Renger JJ (2012) Pharmacological characterization of MK-6096 - a dual orexin receptor antagonist for insomnia. *Neuropharmacology* **62**:978-987.

Yoshida Y, Naoe Y, Terauchi T, Ozaki F, Doko T, Takemura A, Tanaka T, Sorimachi K, Beuckmann CT, Suzuki M, Ueno T, Ozaki S and Yonaga M (2015) Discovery of (1R,2S)-2-{[(2,4-Dimethylpyrimidin-5-yl)oxy]methyl}-2-(3-fluorophenyl)-N-(5-fluoro pyridin-2-yl)cyclopropanecarboxamide (E2006): A potent and efficacious oral orexin receptor antagonist. *J Med Chem* **58**:4648-4664.

Zammit GK (2007) The prevalence, morbidities, and treatments of insomnia. *CNS Neurol Disord Drug Targets* **6**:3-16.

JPET Fast Forward. Published on June 29, 2017 as DOI: 10.1124/jpet.117.241596
This article has not been copyedited and formatted. The final version may differ from this version.

FOOTNOTES

Contact for reprint requests: Alexander Treiber, Idorsia Pharmaceuticals Ltd, Hegenheimermattweg 91, 4123 Allschwil, Switzerland, e-mail: alexander.treiber@idorsia.com

JPET Fast Forward. Published on June 29, 2017 as DOI: 10.1124/jpet.117.241596
This article has not been copyedited and formatted. The final version may differ from this version.

FIGURE LEGENDS

Figure 1 Chemical structures of ACT-541468, ACT-605143 and ACT-658090

Figure 2 Effect of dual orexin receptor antagonists on OxA-induced calcium flux in CHO cells expressing recombinant human OX1 or OX2 receptors. Cells were stained with fluo-4 and pre-incubated with dilution series of antagonists for 120 min followed by the addition of a dilution series of OxA. Peak fluorescence values were converted to CRCs. Data shown are the average of duplicate values (± S.D.) from a representative of at least three experiments. IC_{50} values at 1.6 nM OxA were determined and used as a basis to calculate the apparent K_b via the generalized Cheng-Prusoff equation.

Figure 3 Effect of benzimidazole DORAs on sleep/wake stages at 30 mg/kg in telemetrized rats. Effects of ACT-541468, ACT-658090 and ACT-605143 during the first 6 h of the night-active period in telemetrized male Wistar rats (% of total time). Data are expressed as mean ± SEM, n = 8 per group. *p < 0.05, **p < 0.01, ***p < 0.001 compared to matched vehicle-treated rats; REM, rapid eye movement.

Figure 4 Effect of benzimidazole DORAs on total sleep time (A), latency to non-REM (B) and latency to REM sleep (C) at 30 mg/kg in telemetrized rats**.** Effects of ACT-541468, ACT-658090 and ACT-605143 on (A) total sleep time during the first 6 h of the night-active period (difference vs. vehicle in min for all parameters), (B) on latency to persistent non-REM sleep (in min, first episode of at least 60 s), and (C) latency to persistent REM sleep (in min, first episode of at least 30 s) in telemetrized male Wistar rats. Data are expressed as mean ± SEM, n = 8 per group, *p < 0.05, **p < 0.01, ***p < 0.001 compared to matched vehicle-treated rats.

Figure 5 Dose-response of single oral administrations of ACT-541468 on sleep/wake stages in telemetrized rats over the first 6 h post-dose (A), latency to

JPET Fast Forward. Published on June 29, 2017 as DOI: 10.1124/jpet.117.241596
This article has not been copyedited and formatted. The final version may differ from this version.

persistent non-REM (B) and REM sleep (C) at 10, 30 and 100 mg/kg Effect of ACT-541468 on time spent in active wake, quiet wake, non-REM and REM sleep during the first 6 h of the night-active period (A), on latency to persistent non-REM sleep (in min, first episode of at least 60 sec; B) and on latency to persistent REM sleep (in min, first episode of at least 30 sec, C) in telemetrized male Wistar rats (in min, difference vs. matched vehicle). Data are expressed as mean ± SEM, n = 8 per group. REM, rapid eye movement. *p < 0.05, **p < 0.01, ***p < 0.001 compared to matched vehicle-treated rats.

Figure 6 PBPK and absorption model development and application

Figure 7 Simulated geometric mean plasma concentration (A) and OX2 receptor occupancy (B) vs. time profiles of ACT-541468, ACT-605143 and ACT-658090 after a 25 mg dose to healthy male subjects. Plasma concentration vs. time profiles were predicted using PBPK models (A), and OX_2 receptor occupancy vs. time profiles (B) were predicted based on a E_{max} model driven by the unbound brain concentrations of the benzimidazole compounds.

JPET Fast Forward. Published on June 29, 2017 as DOI: 10.1124/jpet.117.241596
This article has not been copyedited and formatted. The final version may differ from this version.

Figure 8 Observed (daytime and nighttime) and simulated geometric mean plasma concentration vs. time plots of 200 mg almorexant (A) and 40 or 50 mg suvorexant (B) Plasma concentration vs. time profiles were reconstructed based on published data for almorexant (Hoever et al., 2012a) and suvorexant (Sun et al., 2013; Sun et al., 2015). Horizontal lines indicate total plasma concentrations at 8 h after nighttime administration. Data for almorexant are given as geometric mean ± SD with daytime timepoints being shifted by +10 min for clarity. Data for suvorexant are given as geometric means only as no information on variability is given in the published literature.

Figure 9 Observed (daytime and nighttime) and simulated geometric mean plasma concentration vs. time profiles of ACT-541468 after a 25 mg dose administered to healthy subjects. Plasma concentration vs. time profiles were either predicted using PBPK model (simulated) or observed in a clinical trial (daytime and nighttime) (Mühlan et al., 2017). Observed data are given as geometric means ± SD, with daytime time points being shifted by +10 min for clarity.

Figure 10 Adaptive tracking performance of healthy male subjects after a 25 mg dose of ACT-541468. Effect of 25 mg ACT-541468 in an adaptive tracking test in healthy male subjects (n=6) over a period of 10 h post-dosing, expressed as mean change ± SD from baseline, and as compared to placebo (n=2).

JPET Fast Forward. Published on June 29, 2017 as DOI: 10.1124/jpet.117.241596
This article has not been copyedited and formatted. The final version may differ from this version.

TABLES

Table 1 **Mean apparent K_b values for selected dual orexin receptor antagonists in calcium release assays determined in CHO cells expressing human OX_1 and OX_2 receptors ($n \geq 3$)**

Receptor	K_b [σ_g] (nM) [a]				
	Suvorexant	**Almorexant**	**ACT-541468**	**ACT-605143**	**ACT-658090**
Human OX_1	0.68 [2.0]	4.5 [2.3]	0.52 [2.0]	0.62 [1.5]	8.3 [1.2]
Human OX_2	0.42 [1.9]	0.42 [2.2]	0.78 [1.5]	0.70 [1.6]	5.9 [1.4]

[a] K_b values were derived from IC_{50} values using the generalized Cheng-Prusoff equation, and their geometric mean is shown.

JPET Fast Forward. Published on June 29, 2017 as DOI: 10.1124/jpet.117.241596
This article has not been copyedited and formatted. The final version may differ from this version.

Table 2 **Receptor occupancy half-lives of orexin receptor antagonists at human OX_1 and OX_2 receptors as determined by calcium flux measurements after compound wash-out**

Receptor	Parameter[a]	Suvorexant	Almorexant	ACT-541468	ACT-605143	ACT-658090
	$K_{b\_0\ min}$ (nM)	0.87	9.3	0.83	0.14	5.5
Human OX_1	$K_{b\_33\ min}$ (nM)	11	26	13	6.1	104
	$ROt_{1/2}$ (min)	9	22	8	6	8
	$K_{b\_0\ min}$ (nM)	0.48	0.11	1.1	0.34	9
Human OX_2	$K_{b\_33\ min}$ (nM)	18	0.59	224	68	54
	$ROt_{1/2}$ (min)	6	14	4	4	13

[a] K_b values were derived from IC_{50} values using the generalized Cheng-Prusoff equation, and their geometric mean is shown.

JPET Fast Forward. Published on June 29, 2017 as DOI: 10.1124/jpet.117.241596
This article has not been copyedited and formatted. The final version may differ from this version.

Table 3 **Brain partitioning of orexin receptor antagonists in Wistar rats after oral dosing [a]**

Compound	Dose [b] (mg/kg)	Total		Unbound [b]		Ratio
		Brain (nM)	Plasma (nM)	Brain (nM)	Plasma (nM)	
ACT-541468	30	665	685	6.65	19.2	0.3
	100	4010	2840	40.1	79.5	0.5
ACT-605143	30	154	494	1.23	5.93	0.2
	100	2250	1830	18.0	22.0	0.8
ACT-658090	30	614	1050	4.30	9.45	0.5
	100	12000	7270	84.0	65.4	1.3

[a] Geometric mean brain and plasma concentrations were determined at 3 h post-dose (n = 3–4); [b] formulated in PEG400; unbound concentrations in the plasma and brain were calculated using the binding at 1 μM data in **Table 7**.

JPET Fast Forward. Published on June 29, 2017 as DOI: 10.1124/jpet.117.241596
This article has not been copyedited and formatted. The final version may differ from this version.

Table 4 Observed and simulated mean pharmacokinetic parameters of orexin antagonists after oral dosing to Wistar rats and Beagle dogs [a]

Compound	Dose (mg/kg)		$AUC_{0\text{-last}}$ (nM·h)	C_{max} (nM)	T_{max} (h)	F (%)
			Rat			
ACT-541468	10	observed	412	386	0.5	9
		simulated	1376	876	0.6	39
	30 [b]	observed	2950	712	2.3	23
ACT-605143	10	observed	2030	771	1.0	15
		simulated	3140	1670	0.7	43
	30 [b]	observed	6410	1500	1.0	18
ACT-658090	10	observed	4060	2140	0.5	43
		simulated	2610	1360	0.6	38
	30 [b]	observed	7510	1820	0.5	27
			Dog			
ACT-541468	1.6–1.9 [c]	observed	2020	530	1.0	35
		simulated	3480	549	1.2	40
ACT-605143	1.6–1.9 [c]	observed	4740	1720	0.5	28
		simulated	4540	842	1.6	18
ACT-658090	1.6–1.9 [c]	observed	5610	1509	0.25	39
		simulated	7510	978	1.2	40

[a] All compounds were formulated as suspension in 0.5% methyl cellulose. Pharmacokinetic data in the rat and dog are geometric means (n = 3), median is given for $T_{max,}$; [b] formulated in PEG400; [c] dogs received a total dose of 30 mg, bodyweight: 16–18 kg.

JPET Fast Forward. Published on June 29, 2017 as DOI: 10.1124/jpet.117.241596
This article has not been copyedited and formatted. The final version may differ from this version.

Table 5 **Proportion of non-REM and REM sleep relative to total sleep time over the first 6 h period following oral dosing of ACT-541468, ACT-605143 or ACT-658090**

Compound	Dose (mg/kg)	Non-REM (%) [a]	REM (%) [a]
ACT-541468	vehicle	79 ± 3	21 ± 3
	10	78 ± 3	22 ± 3
	vehicle	84 ± 2	16 ± 2
	30	81 ± 2	19 ± 2
	vehicle	85 ± 2	15 ± 2
	100	80 ± 3	20 ± 3
ACT-605143	vehicle	86 ± 2	14 ± 2
	30	78 ± 2 [b]	22 ± 2 [b]
ACT-658090	vehicle	83 ± 2	17 ± 2
	30	81 ± 2	19 ± 2

[a] Data are arithmetic mean ± SEM. All compounds formulated in PEG400 (n=8 per dose group);

[b] $p < 0.001$ compared to matched vehicle-treated animals.

JPET Fast Forward. Published on June 29, 2017 as DOI: 10.1124/jpet.117.241596
This article has not been copyedited and formatted. The final version may differ from this version.

Table 6 Observed and simulated mean systemic pharmacokinetic parameters of orexin antagonists in rats, dogs and healthy subjects [a]

Species	Compound	CL (mL/min/kg)		V_{ss} (L/kg)	
		Observed	Simulated	Observed	Simulated
Rat	ACT-541468	85	104	3.9	2.5
	ACT-605143	32	51	0.8	1.7
	ACT-658090	36	50	3.2	2.5
Dog	ACT-541468	9.5	15	2.4	2.9
	ACT-605143	7.4	7.7	1.1	2.4
	ACT-658090	3.9	4.9	2.2	3.3
Human	Almorexant	8.9[b]	8.1	8.5[b]	8.9
	Suvorexant	0.8[c]	1.0	0.6[c, d]	0.4
	ACT-541468	1.0	1.2	0.4	0.5
	ACT-605143	N/A	0.2	N/A	0.2
	ACT-658090	N/A	0.1	N/A	0.2

[a] Observed pharmacokinetic data are geometric means from n = 3 for rat and dog, and n = 4-20 for healthy human subjects; geometric mean data are given for simulated values; [b] calculated from (Hoch et al., 2012) for a body weight of 80 kg; [c] calculated from (TGA, 2014) for a body weight of 80 kg.

JPET Fast Forward. Published on June 29, 2017 as DOI: 10.1124/jpet.117.241596
This article has not been copyedited and formatted. The final version may differ from this version.

Table 7 Biochemical and physico-chemical data for PBPK model development

Parameter	ACT-541468	ACT-605143	ACT-658090
logD	3.8	4.0	4.3
pK_a	4.2	4.0	4.2
Molecular weight (g/mol)	451	449	490
Solubility FaSSIF (µg/mL) [a,f]	79	76	196 [d]
Solubility FeSSIF (µg/mL) [b]	256	83	653 [d]
Solubility PB (µg/mL) [c]	14	18 [e]	32 [d]
$f_{u,OX2\ assay}$	0.79	0.80	0.69
$f_{u,brain}$	0.010	0.008	0.007
$f_{u,mic}$	0.41	0.34	0.29
Permeability (A-to-B, 10^{-6} cm/sec)	22.6	15.4	34.3
CL_{int} (µL/min/mg, rat)	990	835	988
$f_{u,plasma}$ (rat)	0.028	0.012	0.009
Blood/plasma ratio (rat)	2.1	0.9	0.8
CL_{int} (µL/min/mg, dog)	235	212	89
$f_{u,plasma}$ (dog)	0.024	0.012	0.008
Blood/plasma ratio (dog)	0.7	0.5	0.6
CL_{int} (µL/min/mg, human)	138	149	69
$f_{u,plasma}$ (human)	0.0013	0.0004	0.0010
Blood/plasma ratio (human)	0.5	0.7	0.7

Biochemical data are means of at least triplicate experiments. [a] FaSSIF, simulated intestinal fluid at fasted state, pH 6.5 and 37 °C; [b] FeSSIF, simulated intestinal fluid at fed state, pH 5.0 and 37 °C; [c] PB, phosphate buffer, pH 7.0–7.4, 25 °C; [d] non-crystalline material; [e] at 37 °C; [f] data of hydrochloride salt.

JPET Fast Forward. Published on June 29, 2017 as DOI: 10.1124/jpet.117.241596
This article has not been copyedited and formatted. The final version may differ from this version.

Table 8 Observed and simulated pharmacokinetic parameters and estimated OX_2 receptor occupancy in healthy male subjects [a]

Compound	Dose (mg)	Time of dosing	AUC_{0-24h} (nM·h)	C_{max} (nM)	T_{max} (h)	$T_{1/2}$ [b] (h)	OX_2 occupancy at 8 h (%)
Almorexant	200	daytime	747	182	1.0	2.7	N/A
	200	nighttime	620	74	4.0	6.4	N/A
	200	simulated	1080	157	1.6	3.1	63
Suvorexant	40	daytime [c]	10,500	1130	4.0	12.1	N/A
	50	nighttime [d]	8570	870	3.0	10.8	N/A
	50	simulated	8990	750	3.3	8.7	66
ACT-541468 [e]	25	daytime	5700	1400	1.0	3.0	N/A
	25	nighttime	8270	1050	1.5	5.1	N/A
	25	simulated [e]	6500	814	2.0	4.3	58
ACT-605143	25	simulated	31,900	2380	3.9	10.4	53
ACT-658090	25	simulated	47,500	2660	3.6	26.8	14

[a] Observed and simulated pharmacokinetic data are geometric means, median is given for T_{max}; [b] half-lives were calculated based on the initial decline of the plasma concentration vs. time curves; [c] AUC and C_{max} data were estimated based on data from (Sun et al., 2013); [d] data taken from (Sun et al., 2013); [e] simulated data are for the hydrochloride salt; N/A, not applicable.

JPET Fast Forward. Published on June 29, 2017 as DOI: 10.1124/jpet.117.241596
This article has not been copyedited and formatted. The final version may differ from this version.

FIGURES

Figure 1 Chemical structures of ACT-541468, ACT-605143 and ACT-658090

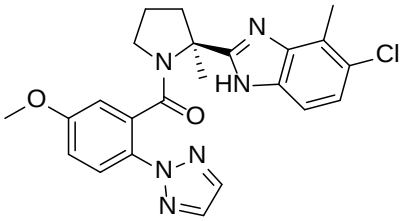

ACT-541468

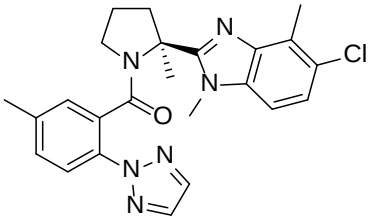

ACT-605143

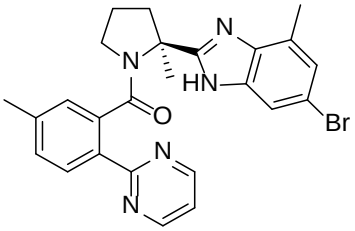

ACT-658090

Figure 2 **Effect of dual orexin receptor antagonists on OxA-induced calcium flux in CHO cells expressing recombinant human OX_1 or OX_2 receptors**

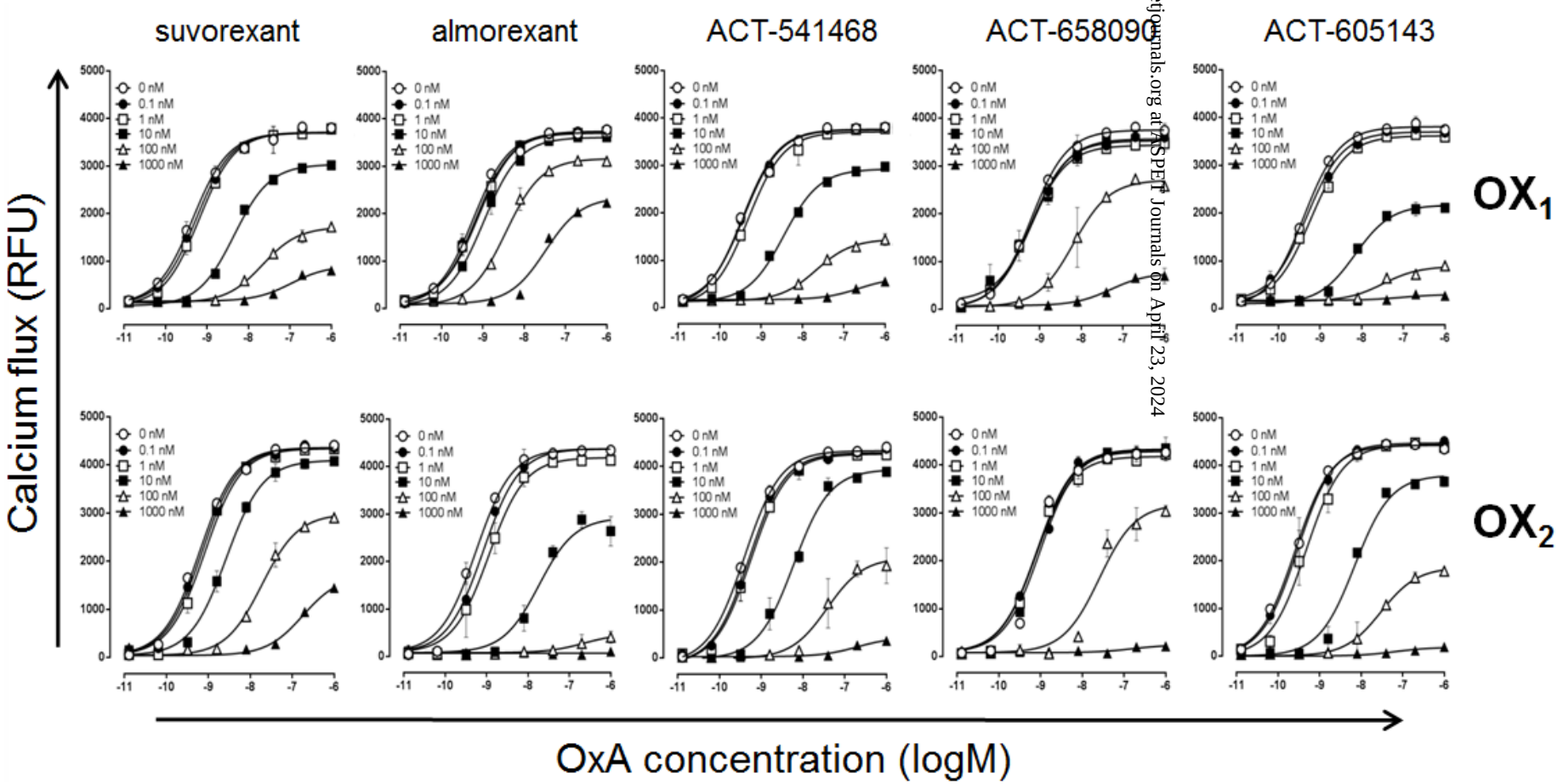

JPET Fast Forward. Published on June 29, 2017 as DOI: 10.1124/jpet.117.241596
This article has not been copyedited and formatted. The final version may differ from this version.

Figure 3 **Effect of benzimidazole DORAs on sleep/wake stages at 30 mg/kg in telemetrized rats.**

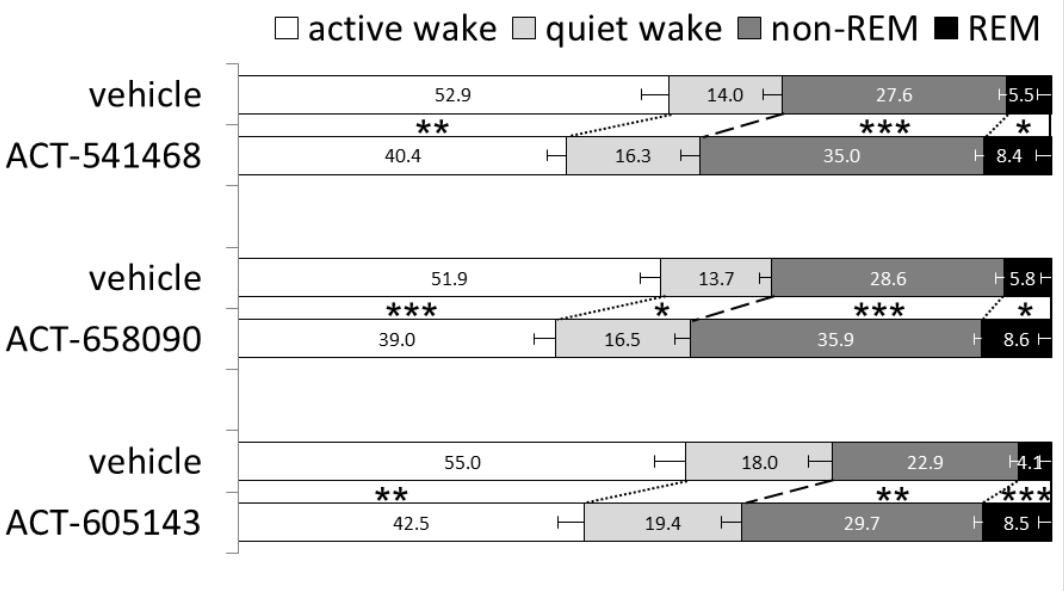

JPET Fast Forward. Published on June 29, 2017 as DOI: 10.1124/jpet.117.241596
This article has not been copyedited and formatted. The final version may differ from this version.

Figure 4 **Effect of benzimidazole DORAs on total sleep time (A), latency to non-REM (B) and latency to REM sleep (C) at 30 mg/kg in telemetrized rats**

A

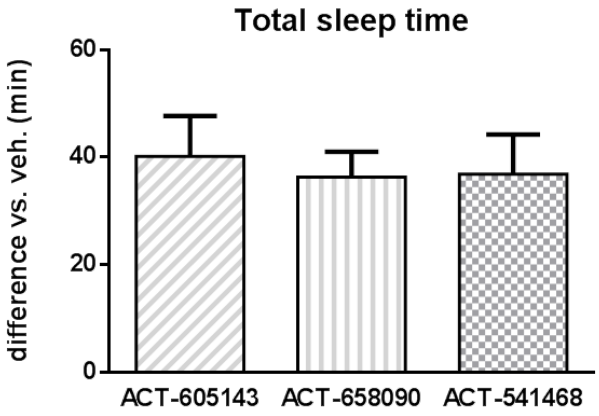

B

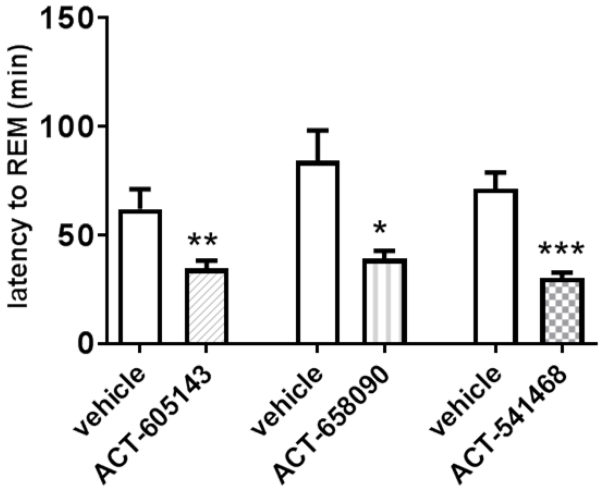

C

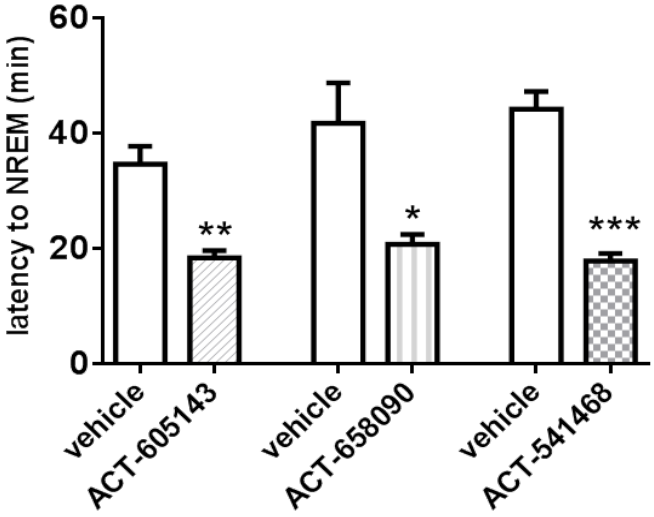

JPET Fast Forward. Published on June 29, 2017 as DOI: 10.1124/jpet.117.241596
This article has not been copyedited and formatted. The final version may differ from this version.

Figure 5 **Dose-response of single oral administrations of ACT-541468 on sleep/wake stages in telemetrized rats over the first 6 h post-dose (A), latency to persistent non-REM (B) and REM sleep (C) at 10, 30 and 100 mg/kg**

A

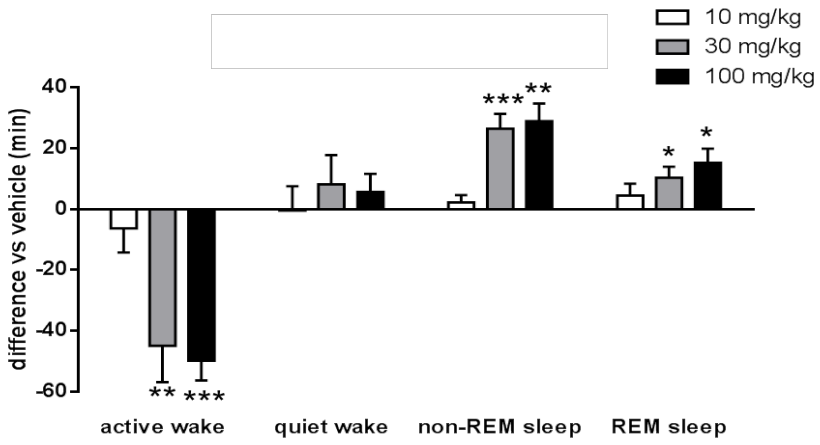

B

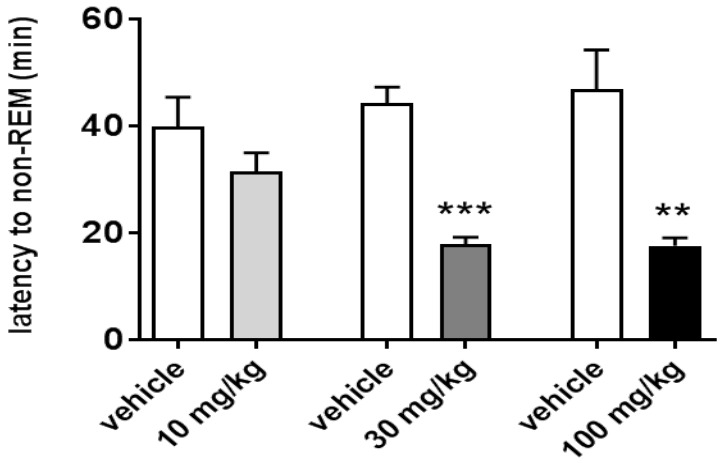

C

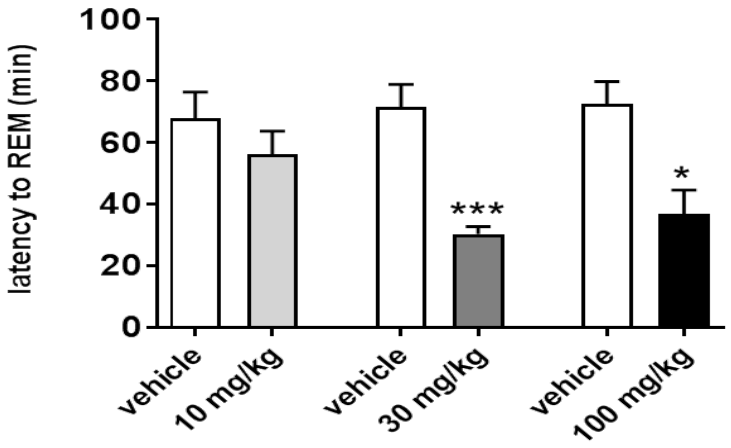

JPET Fast Forward. Published on June 29, 2017 as DOI: 10.1124/jpet.117.241596
This article has not been copyedited and formatted. The final version may differ from this version.

Figure 6 PBPK and absorption model development and application

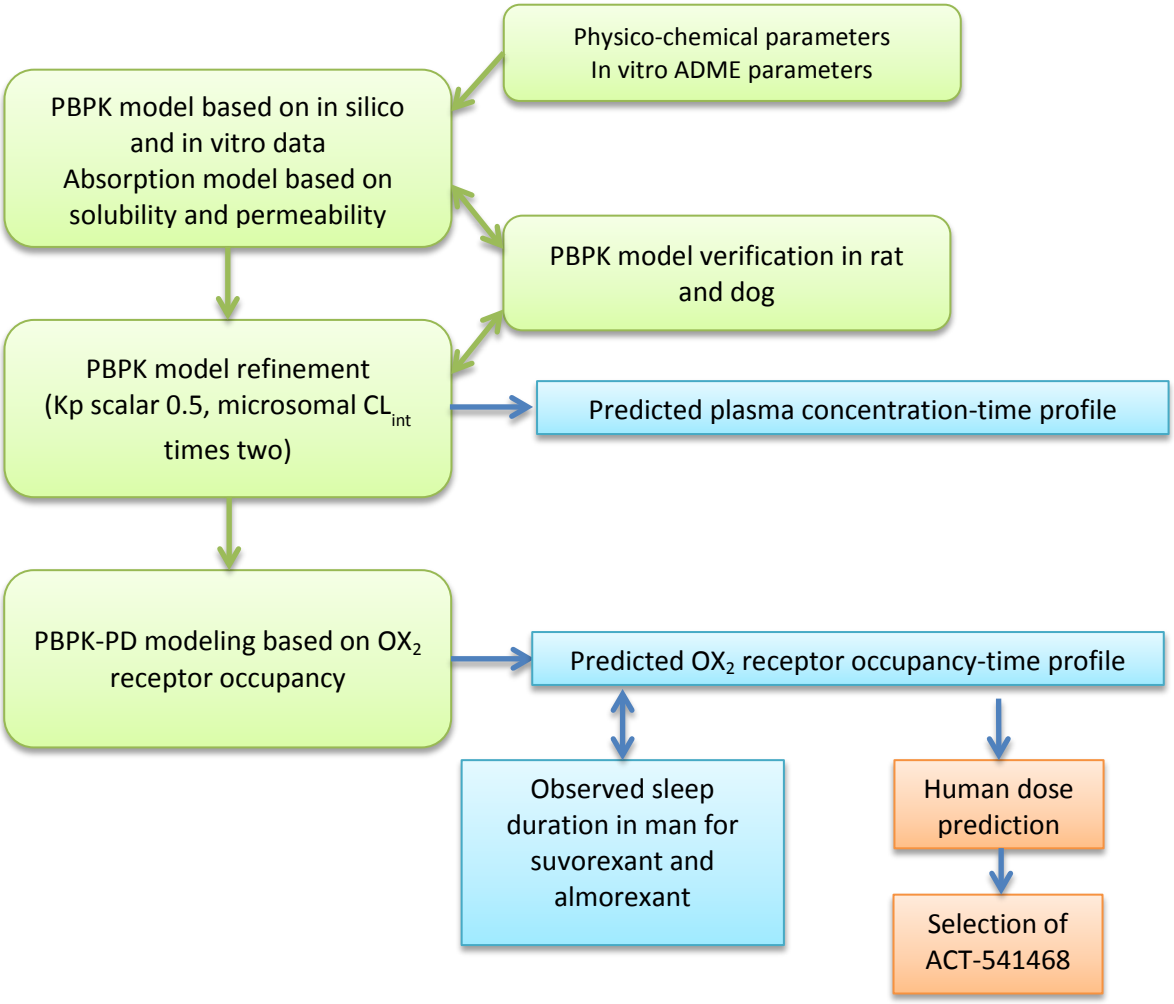

JPET Fast Forward. Published on June 29, 2017 as DOI: 10.1124/jpet.117.241596
This article has not been copyedited and formatted. The final version may differ from this version.

Figure 7 **Simulated geometric mean plasma concentration (A) and OX_2 receptor occupancy (B) vs. time profiles of ACT-541468, ACT-605143 and ACT-658090 after a 25 mg dose to healthy male subjects**

A

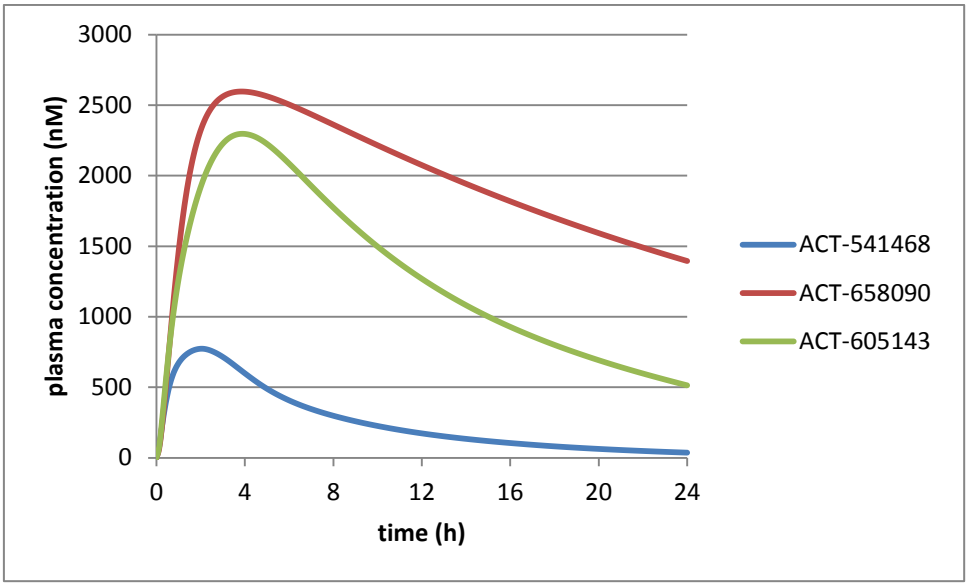

B

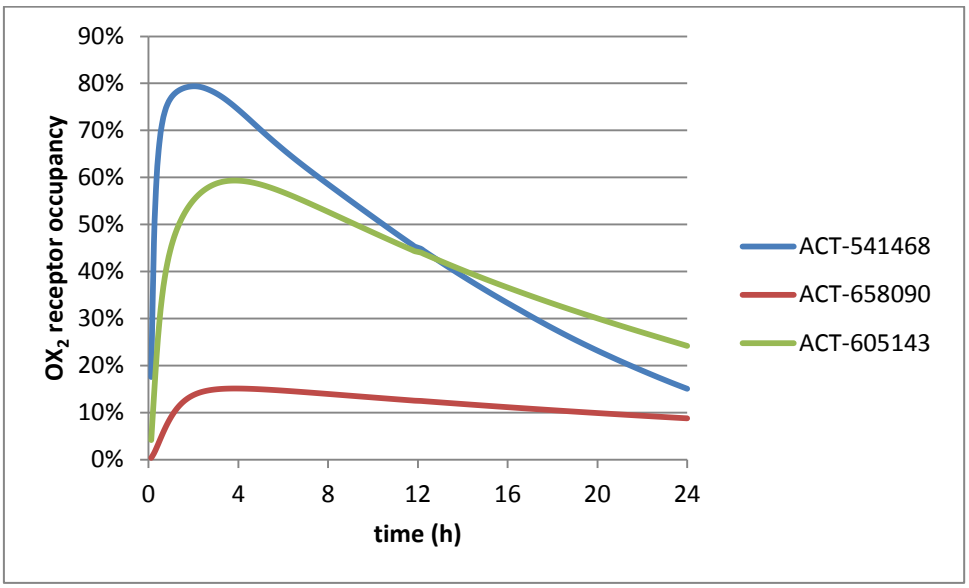

JPET Fast Forward. Published on June 29, 2017 as DOI: 10.1124/jpet.117.241596
This article has not been copyedited and formatted. The final version may differ from this version.

Figure 8 **Observed (daytime and nighttime) and simulated geometric mean plasma concentration vs. time plots of 200 mg almorexant (A) and 40 or 50 mg suvorexant (B)**

A

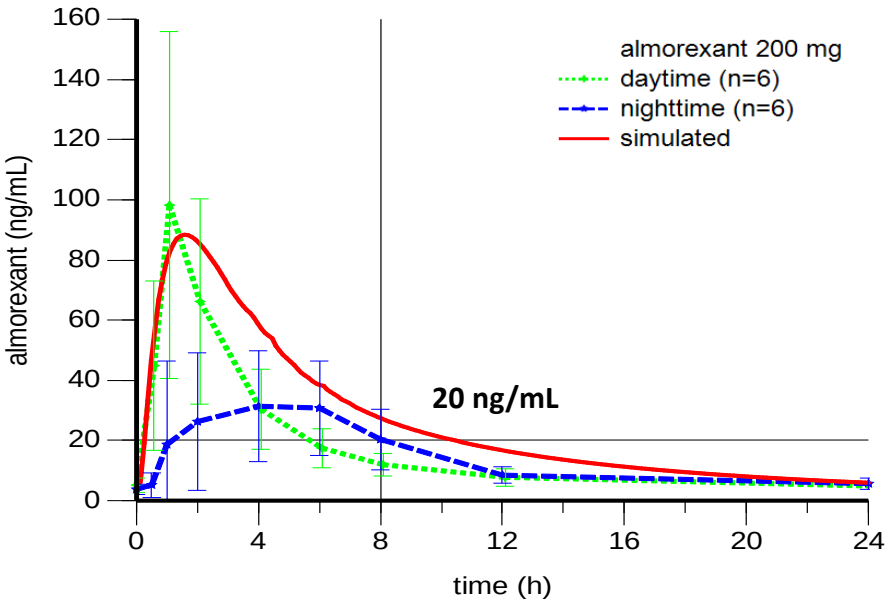

B

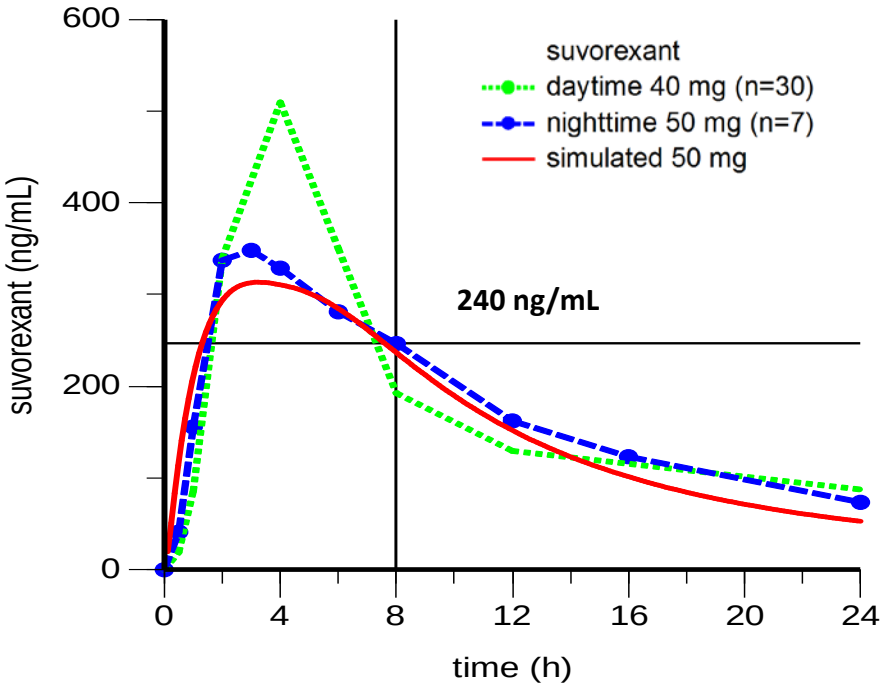

JPET Fast Forward. Published on June 29, 2017 as DOI: 10.1124/jpet.117.241596
This article has not been copyedited and formatted. The final version may differ from this version.

Figure 9 **Observed (daytime and nighttime) and simulated geometric mean plasma concentration vs. time profiles of ACT-541468 after a 25 mg dose administered to healthy subjects**

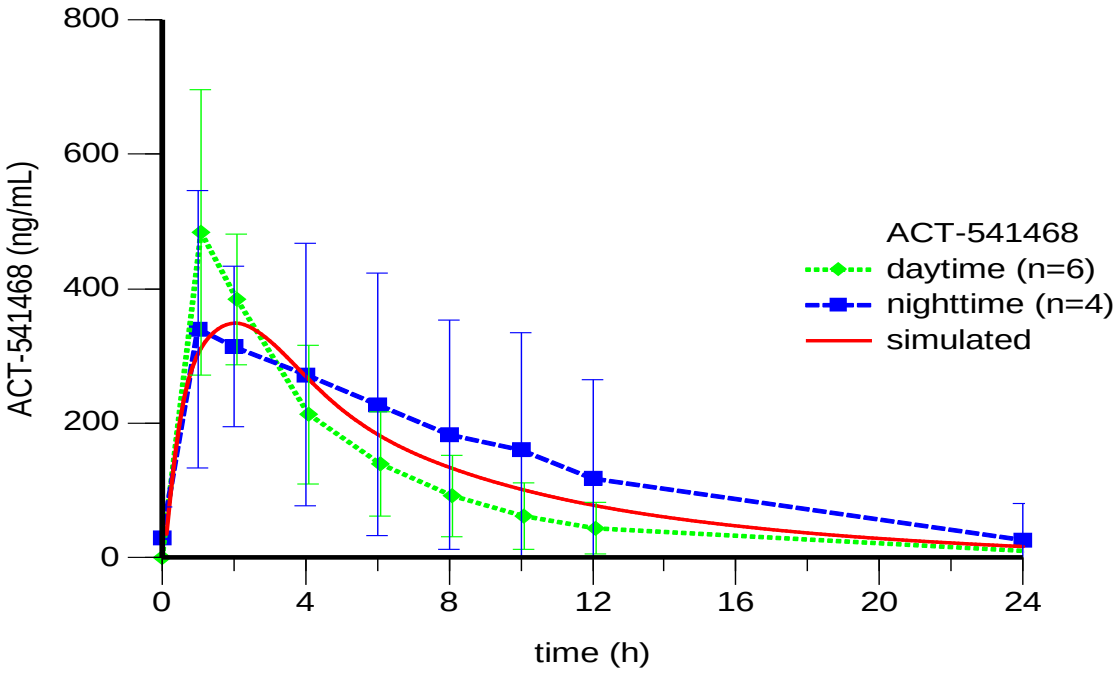

JPET Fast Forward. Published on June 29, 2017 as DOI: 10.1124/jpet.117.241596
This article has not been copyedited and formatted. The final version may differ from this version.

Figure 10 **Adaptive tracking performance of healthy male subjects after a 25 mg dose of ACT-541468**